AD-A121 179 LASER VELOCIMETER MEAUUREMENTS AND ANALYSIS IN TURBULENT FLOWS WITH COMBU..(U) PURDUE UNIV LAFAYETTE IN SCHOOL OF MECHANICAL ENGINEERING 1/1

UNCLASSIFIED W H STEVENSON ET AL. SEP 82 F/G 21/2 NL

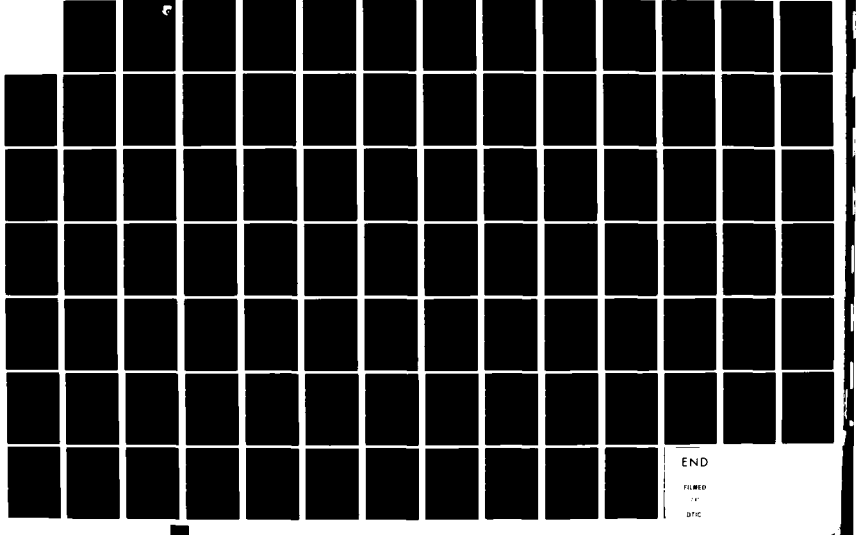

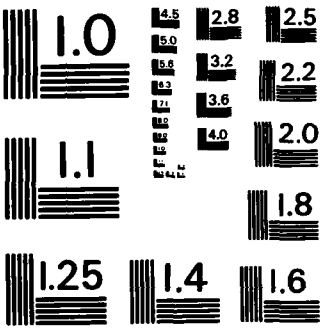

MICROCOPY RESOLUTION TEST CHART
NATIONAL BUREAU OF STANDARDS - 1963 - A

AFWAL-TR-82-2076
Part I

LASER VELOCIMETER MEASUREMENTS AND ANALYSIS IN TURBULENT FLOWS WITH COMBUSTION PART I

W.H. STEVENSON
H.D. THOMPSON
T.S. LUCHIK

SCHOOL OF MECHANICAL ENGINEERING
PURDUE UNIVERSITY
WEST LAFAYETTE, INDIANA 47907

September 1982

Interim Report for Period January 1981 - December 1981

AERO PROPULSION LABORATORY
AIR FORCE WRIGHT AERONAUTICAL LABORATORIES
AIR FORCE SYSTEMS COMMAND
WRIGHT-PATTERSON AIR FORCE BASE, OHIO 45433

NOTICE

When Government drawings, specifications, or other data are used for any purpose other than in connection with a definitely related Government procurement operation, the United States Government thereby incurs no responsibility nor any obligation whatsoever; and the fact that the government may have formulated, furnished, or in any way supplied the said drawings, specifications, or other data, is not to be regarded by implication or otherwise as in any manner licensing the holder or any other person or corporation, or conveying any rights or permission to manufacture, use, or sell any patented invention that may in any way be related thereto.

This report has been reviewed by the Office of Public Affairs (ASD/PA) and is releasable to the National Technical Information Service (NTIS). At NTIS, it will be available to the general public, including foreign nations.

This technical report has been reviewed and is approved for publication.

Roger R. Craig
Project Engineer

Frank D. Stull, Chief
Ramjet Technology Branch
Ramjet Engine Division

FOR THE COMMANDER

James D. Johnson, Col, USAF
Director, Ramjet Engine Division
Aero Propulsion Laboratory

If your address has changed, if you wish to be removed from our mailing list, or if the addressee is no longer employed by your organization please notify AFWAL/PORT, WPAFB, OH 45433 to help us maintain a current mailing list. Copies of this report should not be returned unless return is required by security considerations, contractual obligations, or notice on a specific document.

UNCLASSIFIED

SECURITY CLASSIFICATION OF THIS PAGE *(When Data Entered)*

REPORT DOCUMENTATION PAGE		READ INSTRUCTIONS BEFORE COMPLETING FORM
1. REPORT NUMBER AFWAL-TR-82-2076 Part I	2. GOVT ACCESSION NO. AD-A121179	3. RECIPIENT'S CATALOG NUMBER
4. TITLE *(and Subtitle)* LASER VELOCIMETER MEASUREMENTS AND ANALYSIS IN TURBULENT FLOWS WITH COMBUSTION PART I		5. TYPE OF REPORT & PERIOD COVERED Interim: 1 January 1981 - 31 December 1981 6. PERFORMING ORG. REPORT NUMBER
7. AUTHOR(s) W.H. Stevenson, H.D. Thompson, and T.S. Luchik		8. CONTRACT OR GRANT NUMBER(s) F33615-81-K-2003
9. PERFORMING ORGANIZATION NAME AND ADDRESS School of Mechanical Engineering Purdue University West Lafayette, Indiana 47907		10. PROGRAM ELEMENT, PROJECT, TASK AREA & WORK UNIT NUMBERS 2308-54-01
11. CONTROLLING OFFICE NAME AND ADDRESS Aero Propulsion Laboratory (AFWAL/PORT) Air Force Wright Aeronautical Lab. (AFSC) Wright-Patterson Air Force Base, Ohio 45433		12. REPORT DATE September 1982 13. NUMBER OF PAGES 82
14. MONITORING AGENCY NAME & ADDRESS*(if different from Controlling Office)*		15. SECURITY CLASS. *(of this report)* Unclassified 15a. DECLASSIFICATION/DOWNGRADING SCHEDULE

16. DISTRIBUTION STATEMENT *(of this Report)*

Approved for public release; distribution unlimited

17. DISTRIBUTION STATEMENT *(of the abstract entered in Block 20, if different from Report)*

18. SUPPLEMENTARY NOTES

19. KEY WORDS *(Continue on reverse side if necessary and identify by block number)*

Turbulence measurements
Laser velocimeter
Bias errors (in laser velocimetry)
Recirculating flows
Numerical Analysis

20. ABSTRACT *(Continue on reverse side if necessary and identify by block number)*

Laser velocimeter measurements of mean velocities and turbulence parameters were made in a cylindrical simulated dump combustor. Velocity bias errors were eliminated by use of an experimental technique developed in an earlier study. A comparison of mass flux at different downstream locations based on the measured velocity profiles showed good agreement with the inlet mass flux. The measured mean velocity profiles were in good qualitative agreement with predictions based on the 2/E/FIX computer code, although some disscrepancies in qualitative values due to code limitations were noted.

DD FORM 1 JAN 73 1473 EDITION OF 1 NOV 65 IS OBSOLETE

UNCLASSIFIED

SECURITY CLASSIFICATION OF THIS PAGE *(When Data Entered)*

FOREWORD

This interim technical report was submitted by the School of Mechanical Engineering of Purdue University under Contract No. F33615-81-K-2003 and covers the period 1 January 1981 - 31 December 1981. The research was sponsored by the Aero Propulsion Laboratory, Air Force Wright Aeronautical Laboratories, Wright Patterson AFB, Ohio, under Project No. 2308 with Dr. Roger R. Craig AFWAL/PORT as Project Engineer. Warren H. Stevenson and H. Doyle Thompson of Purdue University were technically responsible for the work.

TABLE OF CONTENTS

LIST OF ILLUSTRATIONS

LIST OF ILLUSTRATIONS (concluded)

LIST OF TABLES

NOMENCLATURE

C_1, C_2, C_D	Turbulence constants
D_m	Digital mantissa
E	Log law constant = 9.0 for smooth walls
f	Doppler frequency
f_s	Net frequency shift
F_R	Fringe spacing
G_k	See Table 1
H	Step height
k	Turublent kinetic energy
m	Number of samples
n	Exponent on TSI processor
N	Number of cycles/burst on TSI processor
r	Raidal coordinate direction
R_1	Outlet radius of sudden expansion
R_2	Inlet radius of sudden expansion
S_Φ	Source term for variable Φ
$(\overline{u'^2})^{1/2}$	RMS streamwise velocity
$\overline{u'v'_\theta}$	Reynolds stress
U_i	Individual velocity realization
U_o	Reference Velocity 25.65 m/s
$\overline{U}$	Mean streamwise velocity
$(\overline{v'^2_\theta})^{1/2}$	RMS circumferential velocity
$\overline{v}_\theta$	Mean circumferential velocity
V	Velocity vector

V_i	Individual velocity realization
x	Streamwise coordinate direction
x_r	Reattachment point

Greek Symbols

Γ	Exchange coefficient
ε	Rate of dissipation of turbulent kinetic energy
θ	Angle between intersecting beams
θ	Circumferential coordinate direction
κ	Log-law constant
λ	Laser wavelength
μ_{lam}	Laminar viscosity
μ_t	Turbulent viscosity
μ_{eff}	Effective viscosity
ρ	Fluid density
σ_ε	Turbulent Prandtl number for ε
σ_k	Turbulent Prandtl number for k
τ_w	Wall shear stress
ϕ	Angle of rotation of the optical system about its axis
Φ	A general variable
ψ	Stream function
ψ^*	Normalized stream function

Math Symbols

Σ	Summation
$\frac{\partial}{\partial x}, \frac{\partial}{\partial r}$	Space derivatives
$\frac{\partial}{\partial t}$	Time derivatives

$\int$	Integral
$\overline{\quad}$, $'$	Time average and its fluctuation

Subscripts

$[\ ]_\phi$	Quantity evaluated at optical rotation angle ϕ

SECTION I

INTRODUCTION

The objective of this research program is to perform laser velocimeter measurements and analysis in turbulent flows with combustion. This report contains the results of the cold flow measurements. Measurements in a similar geometry for combusting flows will be reported in subsequent reports.

The particular flow geometry of interest is that of the axisymmetric sudden expansion. This flow is of interest because the region of recirculation, where a large pressure loss occurs, can be used to advantage as a flame holder for a dump combustor as seen in Figure 1. In the region of recirculation mean velocities are low and the flow is highly turbulent. Because of these flow characteristics, measurements in the recirculation zone have been difficult to obtain with conventional techniques such as hot wire anemometry. With the laser velocimeter (LDV), however, valuable information about such flows can be gained. This instrument has many desirable qualities: no physical probe to intrude on the flow, high spacial and temporal resolution, linear response, and the capability of yielding the direction of the velocity component being measured. The latter feature is particularly important in sudden expansion flows of interest here.

The subject of this investigation is to measure the flow field characteristics in a cold flow axisymmetric, sudden expansion using an LDV, and to determine the accuracy of the data obtained. The experimental data is also compared with a two-dimensional axisymmetric numerical prediction employing k-ε turbulence modeling.

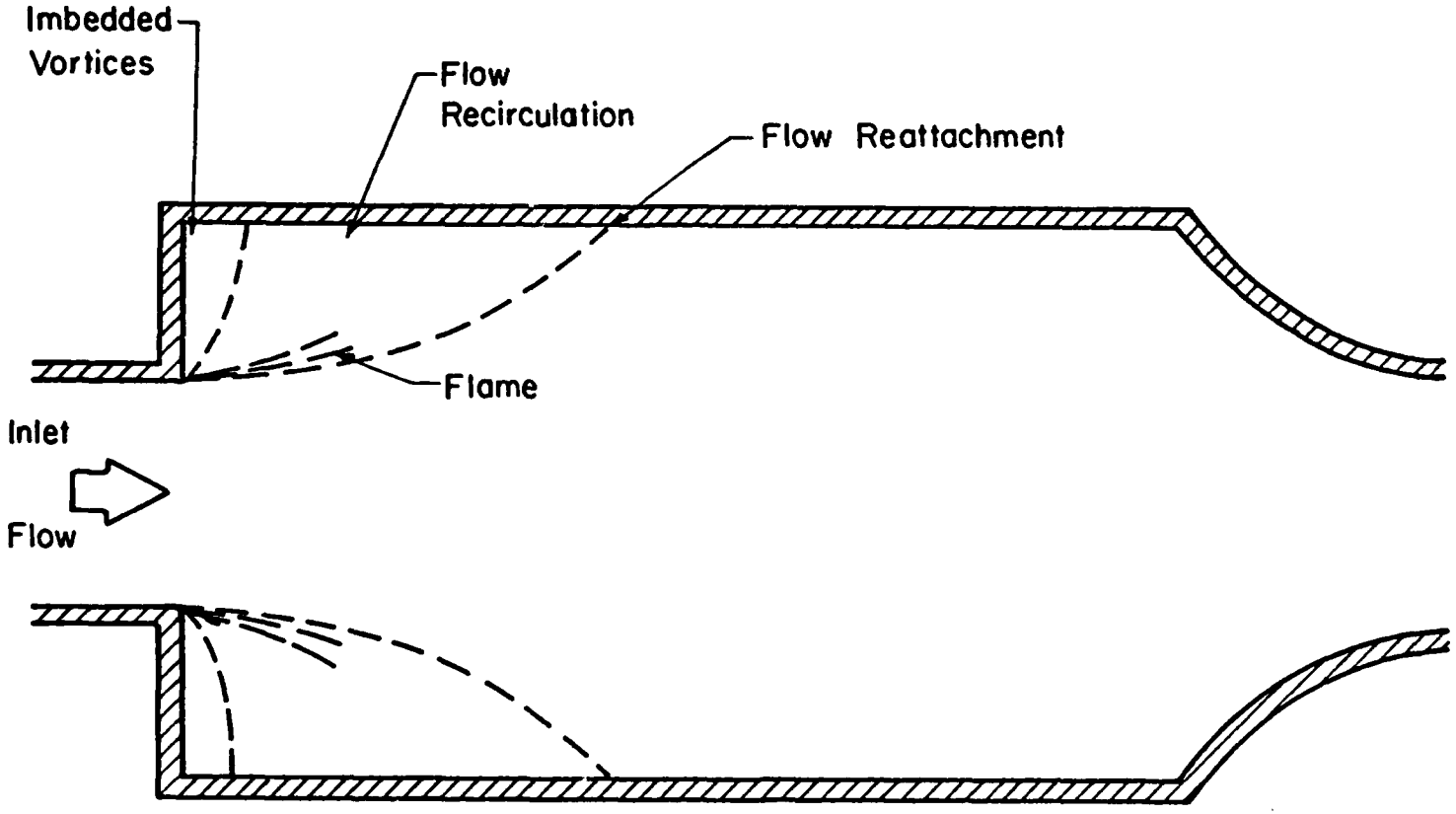

Figure 1 Schematic illustration of dump combustor flow field

Section II gives a review of studies done on this flow field previously along with a review of velocity bias errors in laser velocimetry. Sections III and IV describe the experimental apparatus, measurements and results of the measurements. A description of the numerical code and comparison of the numerical prediction to experimental results is given in Section V. Conclusions and recommendations are presented in Section VI.

SECTION II

LITERATURE REVIEW

1. Introduction

Several studies have been done on flows of the type shown in Figure 1. These studies, both experimental and computational, have been conducted to determine the effect of such parameters as inlet conditions, Reynolds number and step height on reattachment length and the flow characteristics in the shear layer.

Experimenters have used a variety of techniques to study flows of this type including flow visualization, hot wire and hot film anemometry, and most recently, laser velocimetry. The latter technique is most desirable for the reasons stated in Section I.

No instrument is perfect, of course. Two problems which arise when LDV systems are used for turbulent flow studies are incomplete signal bias and velocity bias. These bias errors may affect the accuracy of data obtained by LDV systems using counter type processors. Incomplete signal bias occurs when a seeding particle crosses the probe volume at an angle to the fringe normal and does not cross enough fringes to produce the N Doppler cycles required by the signal processor to validate the output. Thus the data is lost. This problem can normally be minimized by frequency shifting the incoming laser beams.

Velocity bias, on the other hand, is more difficult to handle. This

bias is the result of improper statistical averaging of the velocity data acquired at random times as particles pass through the probe volume. Although several correction schemes have been proposed for the reduction of velocity bias, no one method has as yet been selected as a standard. Since the velocity bias error can be significant in flows of the type involved here, it is an important factor to be considered.

Recent literature dealing with axisymmetric sudden expansions as well as a review of velocity bias will be presented in the following sections.

2. Axisymmetric Sudden Expansions

Macagno and Hung [1], in a laminar flow study, found that symmetric flow patterns existed downstream of a sudden expansion for Reynolds numbers up to 200. Zemmanic and Dougall [2] observed an asymmetric flow pattern for turbulent flow in an axisymmetric sudden expansion, i.e., the reattachment length (as determined by maximum heat transfer) varied arroud the circumference. This is the only reference found which notes such an effect in turbulent flow, however.

Back and Roschke [3] performed dye studies over a range of Reynolds numbers from 20 to 4200. The purpose of the investigation was to study the effect of inlet Reynolds number on shear layer growth and reattachment length. Figure 2 shows that reattachment length had a peak value of 25 step heights for an inlet Reynolds number of 290. In addition, laminar instabilities became visible at this point. When the Reynolds number reached 290, the reattachment length began to rapidly decrease with Reynolds number to a minimum value of approximately seven step

heights when Re≈1000. The reattachment length then slowly increased to a near constant value of approximately nine step heights for Reynolds numbers greater than 3000.

In a comparison of analytical results to experimental data, Teyssandier and Wilson [4] studied the effect of inlet to outlet radius ratio (Beta ratio) on reattachment length and pressure recovery in an axisymmetric sudden expansion. An integral analysis similar to that used for analyzing co-flowing jets was employed in the computational portion of that investigation. They found that pressure recovery varied only slightly with Beta ratio and was predicted quite well by their integral analysis. Reattachment length, on the other hand, was predicted with a reasonable degree of accuracy only for Beta ratios between 0.4 and 0.6.

Freeman [5] performed an experimental investigation of the axisymmetric sudden expansion geometry using an LDV system. In this study Freeman used a one component LDV and restricted measurements to velocity components in the streamwise direction. Figure 3 shows the mean velocity profiles found in the recirculation region. At the inlet to the sudden expansion the flow is that of a developing turbulent pipe flow with a Reynolds number of 30,000 based on centerline velocity and step height. The maximum (negative) recirculation velocity was approximately 10% of that on the centerline and occurred one exit pipe diameter downstream of the step face. Figure 4 shows stream function contours from which a reattachment length of 8.78 step heights was obtained. Freeman concluded that the LDV yielded data that was as good as data obtainable with hot wire anemometry as well as giving the direction of the velocity component being measured.

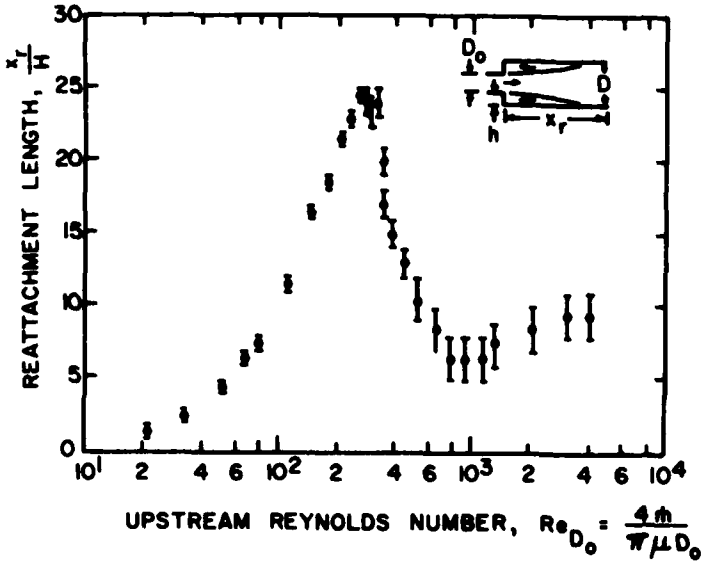

Figure 2 Reattachment length, x_r/H as a function of upstream Reynolds number (from Back and Roschke [3])

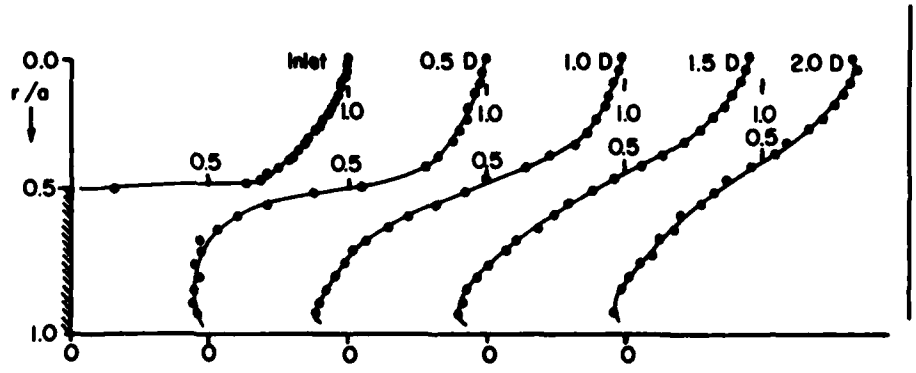

Figure 3 Mean velocity profiles in recirculation region (from Freeman [5])

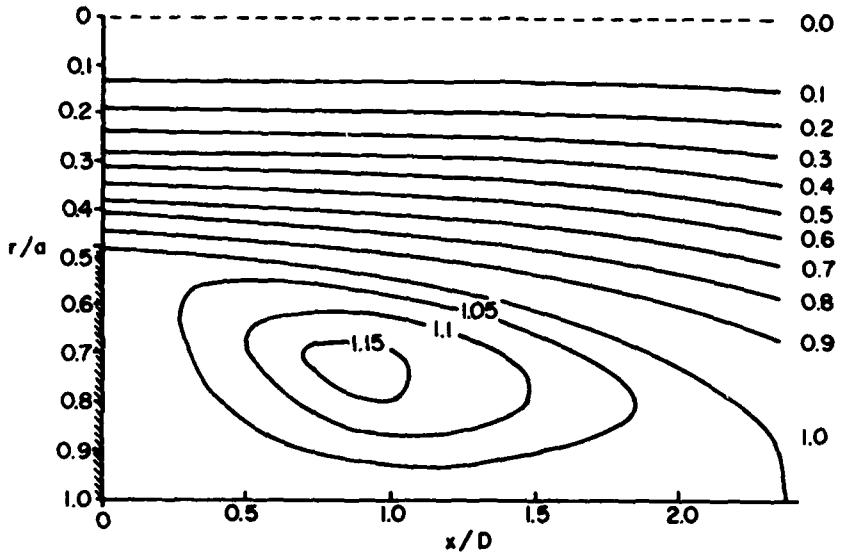

Figure 4 Normalized stream function contours (from Freeman [5])

Gosman, Khalil and Whitelaw [6] performed a numerical investigation of axisymmetric sudden expansions using the two-dimensional time averaged Navier-Stokes equations along with k-ε turbulence modeling. They found that the k-ε turbulence model, although sufficient for engineering purposes, did not provide an accurate representation of the flow field. The dissipation equation was believed to be the major contributing factor in the deficiency of this model. Although more complex turbulence models have been developed, the k-ε model appears to predict the flow field as well as any of the other large scale models they investigated.

An experimental study was performed by Drewry [7] on the axisymmetric sudden expansion in a ramjet combustor using flow visualization techniques, pressure measurements, and gas sampling in the combusting flow field. Drewry found that the reattachment length varied linearly

with step height. He also found that a circumferential flow existed downstream of the sudden expansion regardless of inlet flow swirl and that there was a direct correlation between cold flow mixing and combustion efficiency as a function of reattachment length.

In 1977 a series of LDV measurements were made by Moon and Rudinger [8] on an axisymmetric annular sudden expansion. Experimental data were obtained using both a one color-one component and a two color-two component system. The advantage of the latter is that mean velocities and turbulence parameters may be obtained directly whereas the former requires indirect calculations using single component measurements. Although their system had two component capability, only mean streamwise velocities were then compared with analytical predictions using a modified version of the SIMPLE computer code. They, like Freeman, found that the LDV had unique advantages which made it desirable for studying recirculating flows. Figure 5 shows data obtained in their study along with data obtained in previous studies for reattachment length as a function of inlet Reynolds number. The data was interpreted as showing that reattachment length had no functional dependence on Reynolds number for turbulent flows. They also found that the flow downstream of the sudden expansion was symmetric, thus contradicting the speculation of Zemmanic and Dougall based on experimental results in a two-dimensional flow. The computational predictions of Moon and Rudinger were claimed to give good agreement with the experimental data although only one velocity profile comparison, shown in Figure 6, was presented.

Kankovi and Page [9], using pressure taps and hot wire anemometry, found that reattachment occurredin the vicinity of eight step heights downstream of the sudden expansion. They also noted the presence of

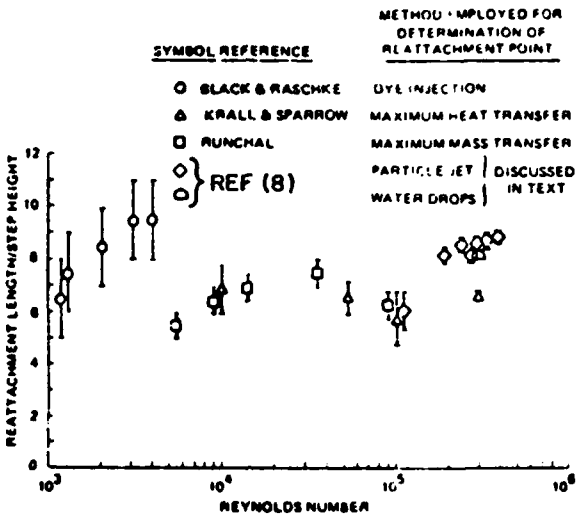

Figure 5 Variation of reattachment length with Reynolds number (from Moon and Rudinger [8])

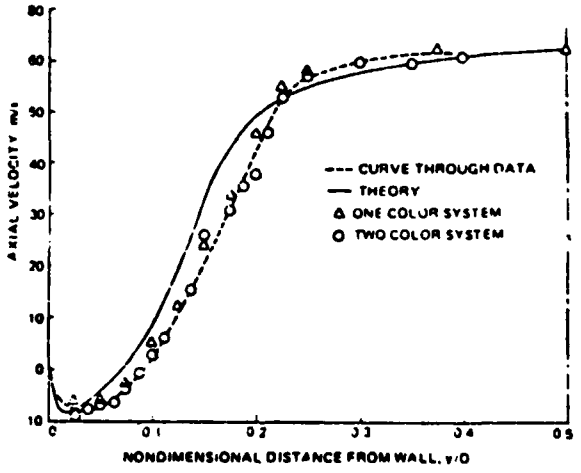

Figure 6 Comparison of predicted and measured velocity profiles (from Moon and Rudinger [8])

a weak secondary separation point located within one step height of the sudden expansion.

A review of the studies described above shows that the observed reattachment length varies between 6 and 11 step heights. Although this was noted by the experiments, little has been done to determine the reason for this wide variation. Keuhn [10] suggested that part of the variation can be attributed to differences in the inlet conditions, but that most may be due to an adverse pressure gradient effect. He showed that superimposing different pressure gradients on the sudden expansion flow field, keeping inlet conditions constant, led to large variations in reattachment length.

3. Velocity Bias

The problem of velocity bias has been studied by numerous investigators over the past eight years, often with conflicting results. In this section a few of these studies will be briefly reviewed to illustrate the various approaches which have been used. A more complete discussion can be found in [11].

McLaughlin and Tiederman [12] presented the first open literature discussion of the velocity bias effect which results from simple averaging of the data obtained with counter type processors. Since, in a uniformly seeded flow, more particles will be carried through the LDV probe volume per unit time during periods when the velocity is high than when it is low, one expects the ensemble average velocity to be higher than the true mean velocity. The problem will occur only in turbulent or time dependent laminar flows.

McLaughlin and Tiederman suggested a correction scheme to minimize

velocity bias. They proposed that for a spherical probe volume, the mean velocity, $\overline{U}$ and RMS velocity $\sqrt{\overline{u'^2}}$ would be given by

$$\overline{U} = \frac{\sum_{i=1}^{m} \frac{1}{|V_i|} U_i}{\sum_{i=1}^{m} \frac{1}{|V_i|}} \tag{1}$$

$$\sqrt{\overline{u'^2}} = \left[\frac{\sum_{i=1}^{m} \frac{1}{|V_i|} (U_i - \overline{U})^2}{\sum_{i=1}^{m} \frac{1}{|V_i|}} \right]^{1/2} \tag{2}$$

where $\overline{U}$ is the mean velocity, $\sqrt{\overline{u'^2}}$ is the RMS velocity, the U_i are the individual velocity samples for the streamwise component and the $|V_i|$ are the magnitudes of the instantaneous velocity vector. Since the magnitude of the instantaneous velocity vector is not known, McLaughlin and Tiederman proposed replacing it by the magnitude of the velocity component in the mean direction. Although this correction scheme works fine for low turbulence level flows, it tends to over correct the mean velocity in highly turbulent flows which have large velocity components perpendicular to the mean flow direction as, for example, in sudden expansions.

Barnett and Bentley [13] believed that velocity bias could be eliminated by using harmonic averaging of the individual velocity realizations. Their correction for the mean velocity was given by

$$\overline{U} = \frac{1}{T} \sum_{i=1}^{m} U_i \Delta t_i \tag{3}$$

where $\overline{U}$ is the mean velocity, the U_i are the individual velocity reali-

zations, Δt_i is the time between velocity realizations and T is the total time interval for sampling. In addition they believed that in uniformly seeded flows where the particle arrival rate is much lower than the frequency of turbulent oscillation, no velocity bias would exist. However no data were shown to support this theory.

Hoesel and Rodi [14] noted that the correction scheme proposed by McLaughlin and Tiederman was too restrictive because it required that the flow be uniformly seeded. They suggested two correction schemes. For uniformly seeded flows the LDV measurements were weighted with particle residence time and for non-uniformly seeded flows the LDV measurements were weighted with the particle separation time. There was no attempt to compare their data with independent data. Thus no conclusions can be drawn as to the accuracy of this correction scheme.

Dimotakis [15] showed that bias-free data could be obtained if both the velocity and residence time for the individual particles were known. Along with this, the sampling frequency had to be higher than the frequency of turbulent oscillations.

Durão, et. al. [16] experimentally found that the Doppler frequency varied with particle arrival time. They suggested that weighting the individual velocity realizations with particle arrival time would eliminate the problem of velocity bias. Unfortunately there was no mention of how particle arrival time was defined or determined.

In an earlier paper Durão and Whitelaw [17] observed that there was an inverse dependence of signal amplitude and visibility on particle velocity. This implies a bias which is opposite in nature to velocity bias. Two sets of data were taken in this investigation. In both cases

it was shown that maximum signal amplitude decreased with increasing particle velocity (Figure 7). They also noted that signal visibility varied with particle velocity and that zero visibility could be obtained. However, an indirect method was used to obtain these results and it is not clear that this effect would actually exist in practice.

Roesler, et al. [11] proposed that by using the proper sampling technique velocity bias could be eliminated. This technique consisted of having particle arrival rate in excess of 5000 particles per second and sampling at a much lower rate. By doing this Roesler showed that data would be sampled at nearly equal time increments which should yield a true time average. The experimental results indicated a bias error which agreed with that predicted by McLaughlin and Tiederman at low turbulence levels but differed substantially at turbulence intensities above 20 percent as expected. This study demonstrated conclusively that the method of data sampling affected the measured mean velocity in the expected manner.

McDougall [18] suggested a correction scheme which was based on a theoretically based probability density function. This function was formed using three-dimensional Gausian statistics and the number of measurements per second. He showed that with only reasonable estimates of $V/(\overline{v^2})^{1/2}$ and $(\overline{u^2})^{1/2}/(\overline{v^2})^{1/2}$ a theoretical debiasing scheme could be formulated for measurements with a one component LDV. The results of this correction scheme were then compared with data for which the sampling rate was high enough to supposedly define the complete velocity-time history. He found that the mean streamwise velocities determined using his correction scheme were within two percent of those computed from the data. However, the results for RMS velocity were less impressive,

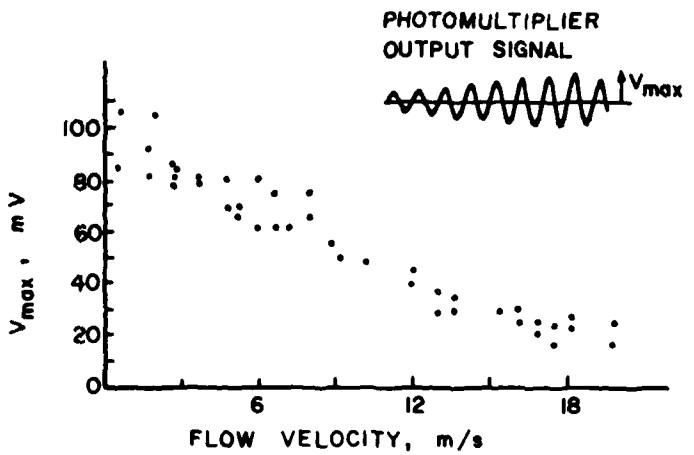

Case i

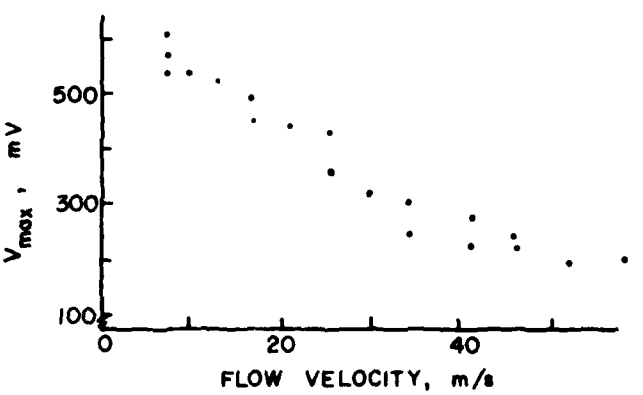

Case ii

Figure 7 Maximum signal amplitude variation with velocity (from Durão and Whitelaw [17].)

with the correction scheme yielding results 10 percent and more under the values obtained from the measurements.

Since the experimental bias elimination scheme of Roesler et al. appears to give results for mean velocity which are free of bias, it is a logical choice in cases where it can be implemented. The methods which require simultaneous time and velocity information are also acceptable, but time data is often not available with standard signal processors.

SECTION III

EXPERIMENTAL APPARATUS

1. Introduction

The LDV used in this investigation was designed specifically to allow investigation of the effect of data acquisition methods and optical parameters on measurements in highly turbulent flows. The system allowed for variation in LDV optical parameters, seeding particle arrival rate and data sampling conditions. The apparatus may be divided into four major subsystems:

1) The LDV
2) The Flow System
3) The Data Acquisition System
4) The Seeding System

2. The LDV

The LDV used is a one color-one component system. It has the capability of changing the size of the probe volume, fringe spacing and angular orientation of the probe volume. These features allow matching the LDV optical parameters to the flow geometry. The general layout of the LDV is shown in Figure 8.

Laser light for the system is provided by a five watt Coherent Radiation Model 52 argon ion laser normally operated on the green line (.5145 μm). The laser beam first passes through a polarization rotator

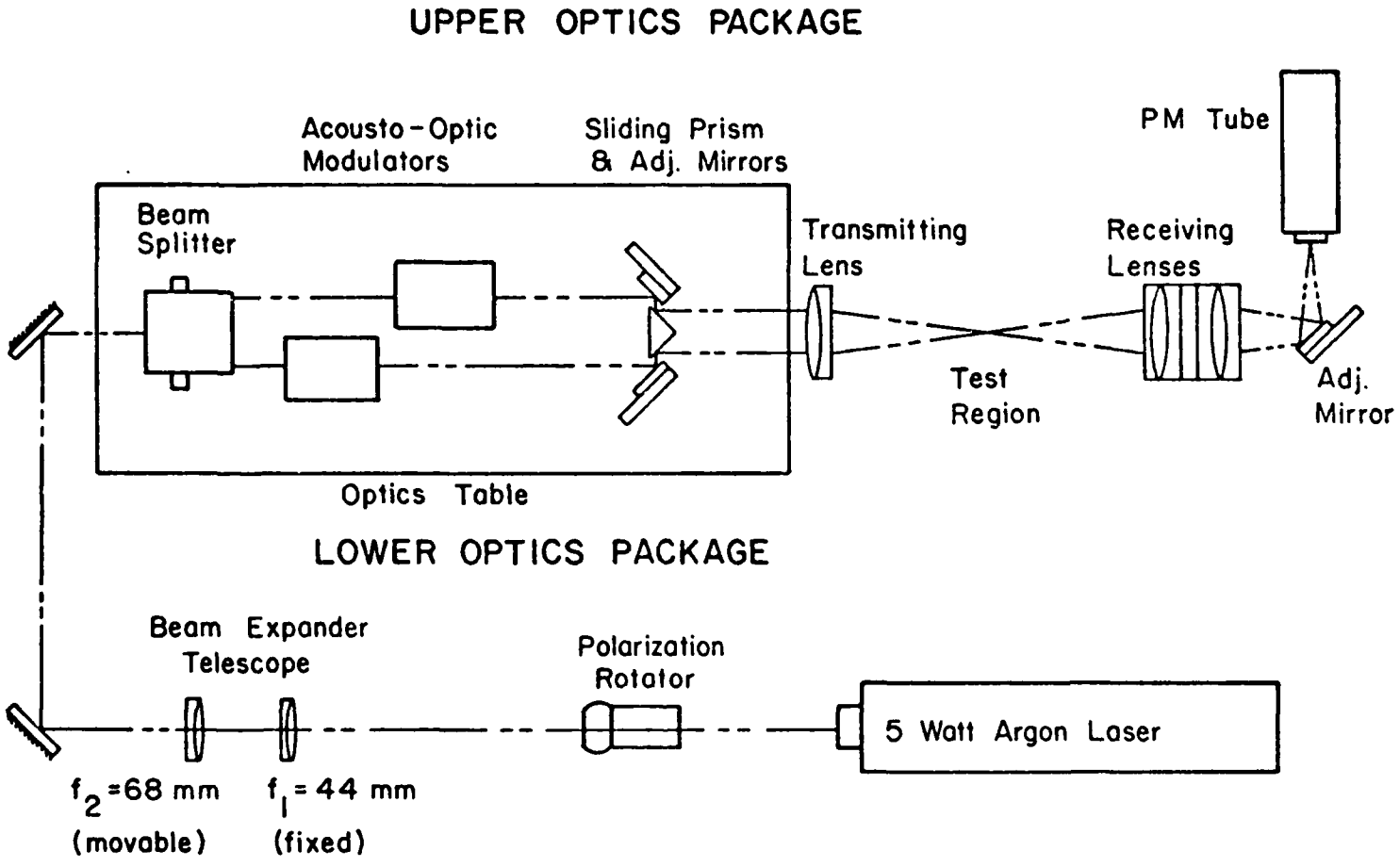

Figure 8 LDV optics package

which insures maximum fringe contrast in the probe volume. The beam is collimated by a series of two lenses which can be adjusted to control the beam diameter. A beam splitter then divides the beam into two parallel beams of equal intensity which enter two acousto-optic modulators. These modulators shift the frequency of each incoming beam by an amount equal to that of the driver. The frequency shift may be either up or down allowing for a wide range of net frequency shifts between the two beams. A net frequency shift of 10 MHZ was used in the present study.

Upon leaving the modulators, the beams are reflected by adjustable mirrors to a sliding prism. Adjustment of the prism changes beam separation and therefore the converging beam angle, thus controlling the fringe spacing and number of fringes in the probe volume. The adjustable mirrors are used to position the beams such that they cross at their waists on the optical axis after passing through the transmitting lens. The transmitting lens has a focal length of 250 mm.

The receiving lenses are a 250 mm lens and a 120.6 mm lens mounted several centimeters apart. The receiving lenses and the entire receiving optics package may be adjusted along the optical axis for rough adjustment of the probe volume image on the pinhole mounted in front of the photomultiplier tube. Fine focusing is available through the use of an adjustable mirror and a fine threaded pinhole housing.

The transmitting optics package is mounted on bearings which allow angular rotation about the optical axis and thus permit any velocity component in a perpendicular plane to be measured. The entire optics package is mounted on a milling machine bed which can be electrically motored in any of the three cartesian directions within $\pm$0.1 mm thus giving precise location of the probe volume inside the test section. A

more detailed description is given by McVey [19].

3. Flow System

The LDV system used in this investigation required a flow system which has easy optical axis. The geometries used in this study were that of an axisymmetric sudden expansion and a two-dimensional converging nozzle. The two-dimensional nozzle provided a broad velocity range in which the effect of velocity on signal amplitude could be investigated. The flow system consisted of five major parts, as shown in Figure 9:

1) A radial vane blower
2) A flow conditioning section
3) A connecting duct
4) A test section
5) An extension duct

The radial vane blower was a Peerless model PWB4GA driven by a variable speed direct current motor. The blower-motor combination allows a capacity of 1100 cfm.

The flow conditioning section consisted of a set of flow straighteners 95.25 mm in diameter for the axisymmetric sudden expansion and 101.6 mm square for the two-dimensional nozzle. The elements of this section included wire window screen followed by a honeycomb of 6.35 mm diameter soda straws 25.4 mm in length. This section exited to a series of four window screens spaced 25.4 mm apart. The section was 152.4 mm in length and was connected to the blower via a convergent adapter.

Downstream of the flow conditioning a connecting duct connected the test section to the flow conditioning section. The connecting duct was 1206.5 mm long for the axisymmetric case and 314.4 mm long for the two-

dimensional nozzle case.

The annular test section consisted of two parts; a flow nozzle and a 95.25 mm diameter duct both made of commercial grade clear Plexiglass. The flow nozzle was 25.4 mm long and had a radius ratio of R_1/R_2=1.875. The nozzle exhausted into a 95.25 mm diameter duct which was 508.0 mm long. This combination created the sudden expansion effect. A cross sectional view of this test section is shown in Figure 10. The actual test region was 482.6 mm long and lined with a series of pressure taps spaced 25.4 mm apart. Additional pressure taps every 127.0 mm located at $\pm$ 60° relative to those mentioned previously allowed a check for flow symmetry.

The two-dimensional nozzle test section used was 152.4 mm high at the inlet and 371.0 mm long with a 6.7° semi-angle. This test section was also made of commercial grade clear Plexiglass.

In both cases the test sections exhausted into a 1701.8 mm long extension duct. An exhaust fan located 1523.0 mm downstream of the extension duct exit was used to remove particle laden air from the room.

4. Data Collection, Storage and Processing

The photomultiplier tube output was fed into a Thermo-Systems Incorporated (TSI) Model 1980 signal processor [20]. This unit features a 250 MHZ clock with two nano second resolution and capability of either digital or analog output; only the digital output was used in this investigation. The processor data rate (number of validated velocity measurements per second) depends on the rate at which seeding particles enter the probe volume, the processor gain setting (which effectively sets the trigger level) and the required number of cycles per Doppler

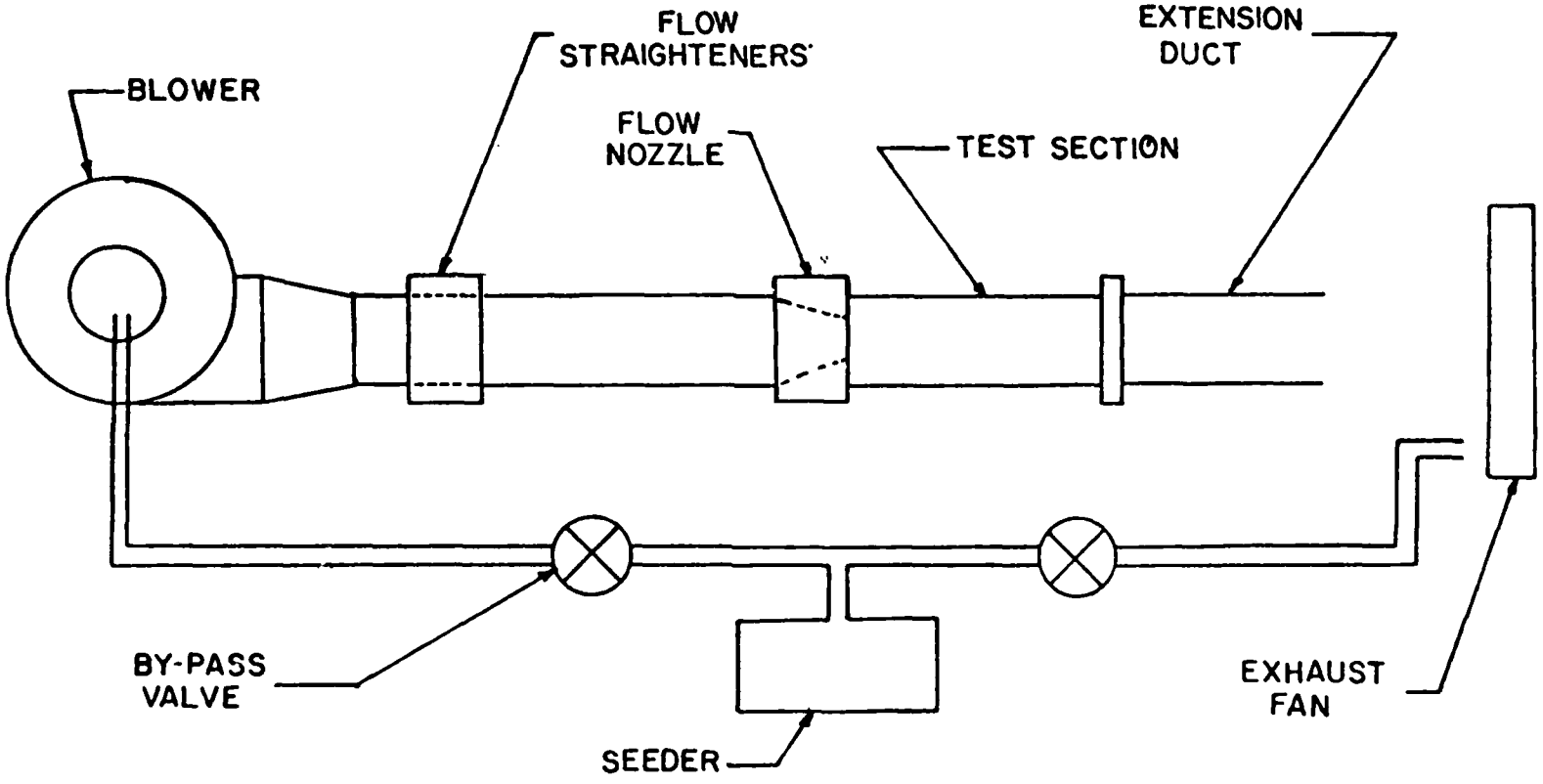

Figure 9 Flow system

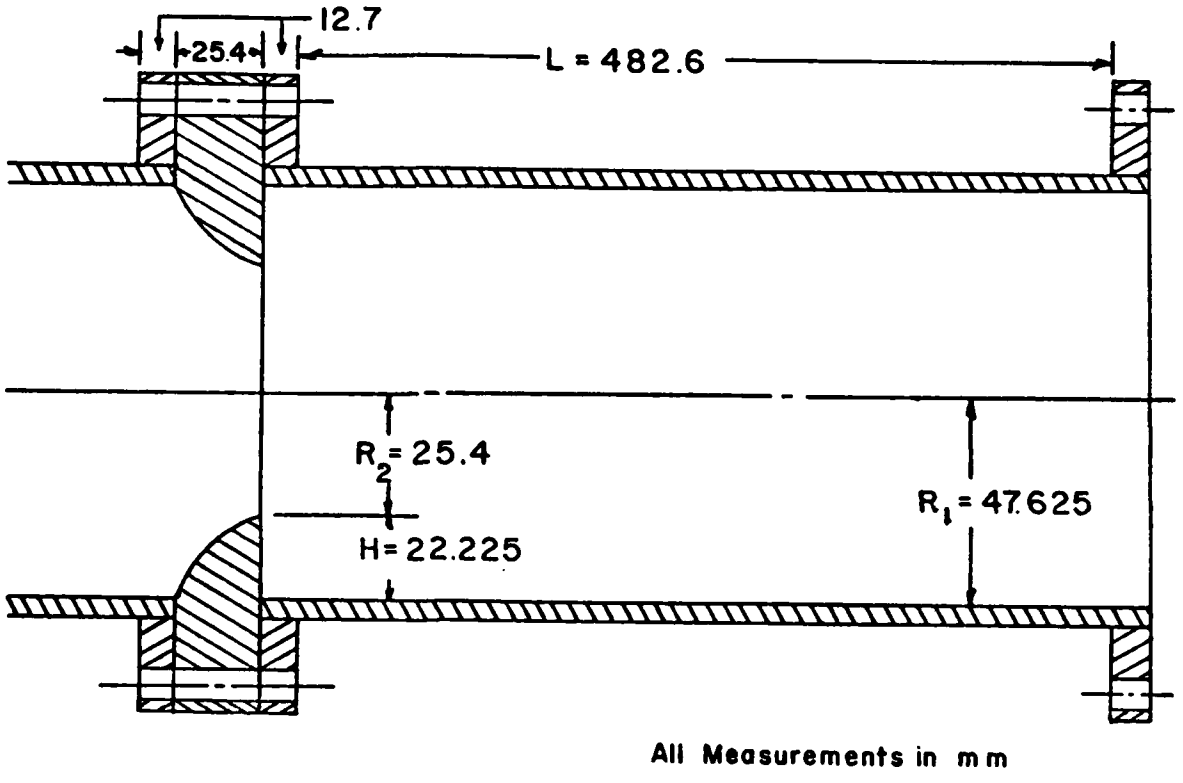

Figure 10 Geometry of axisymmetric test section

burst. Data rates as low as a few per second to in excess of 30,000 per second were obtained. The rate at which particles enter the flow section was controlled by a bypass valve between the seeding generator and a dump tube which sent excess particles directly to the exhaust fan.

Data acquisition and short term storage were performed by an IMSAI 8080 microcomputer and Micropolis floppy disk system. Data could be sampled from rates as low as 0.1 sample per second to approximately 4800 samples per second. The microcomputer had the capability of storing 9500 data points in its memory. After sampling the data was written onto a floppy disk for temporary storage. Each disk is capable of storing 100,000 data points. The microcomputer also interfaced with Purdue University's CDC 6500 and 6600. Data may be transferred from the floppy disk to magnetic tape for permanent storage. The CDC 6500 and 6600 were used for all data reduction.

The microcomputer and TSI processor were also interfaced so that the velocity sampling was jointly controlled by the processor and the microcomputer. When the TSI processor has a data point ready, it transmits a data ready pulse to the microcomputer. Upon reception of the data ready pulse the microcomputer returns a data inhibit pulse to the TSI processor. The inhibit stops the TSI processor from accepting more data and causes it to hold the present data until it can be read. The microcomputer waits a fixed amount of time, chosen by the operator, before reading the data point. After the data is read the data inhibit is removed by the microcomputer and the cycle continues until the desired number of samples has been taken. The rate at which data is actually taken is therefore controlled by the slower of the two instruments.

5. The Seeding System

The seeder was one which is commercially built by TSI. It consisted of Model 3074 air supply, a Model 3076 liquid atomizer and a Model 3072 evaporation-condensation monodisperse aerosol generator. This system produced seeding particles not greater than 1.0 micron in diameter using a solution of 100% Dioctyl Phthalate (DOP). The seeder was operated at constant pressure, normally 60 psi, while the evaporation-condensation unit was operated at a constant voltage, 60 volts. The seed density inside the flow channel was controlled by means of the by-pass valve. When the by-pass valve was open seeding particles were allowed to by-pass the flow channel going directly to the exhaust fan. Operation in this manner allowed the seeding density in the test section to be varied over a wide range without disturbing the seeding system.

SECTION IV

EXPERIMENTAL RESULTS

1. Introduction

Mapping of the axisymmetric annular sudden expansion flow field required both direct measurements and indirect computations relating the direct measurements to various turbulence parameters. The flow and turbulence parameters obtainable were:

1) Mean velocities $\bar{U}$ and $\bar{v}_\theta$
2) Turbulence parameters $(\overline{u'^2})^{1/2}$, $(\overline{v_\theta'^2})^{1/2}$; $\frac{1}{2}(\overline{u'^2}+\overline{v_\theta'^2})$, $\overline{u'v_\theta'}$
3) Integrated mass flow rate
4) *Reattachment length*

No information about radial flow parameters was obtained since measurements were limited to the horizontal axis of the annular tunnel. There are two reasons for this. One is the intensity difference between the two beams due to the partial reflection effects when the beams are not symmetrically incident on the curved tube. More significant is the asymmetric refraction of the two beams which occurs when the are not symmetrically incident. As a result of this the beams do not cross at their waists nor do they cross in the plane of the transmitting optics. This latter reason causes distortion of the probe volume, makes precise location of the probe volume in the test section difficult and impares signal reception by the receiving optics.

In addition to the set of measurements noted above, a series of mea-

surements was taken to determine the effect of velocity bias on integrated massflow rate at several axial locations. The various measurement techniques employed in this investigation along with the results of the measurements are presented in the following sections.

2. Mean Velocities and Turbulence Parameter Measurements

2.1 Measurement Technique

All mean velocities and turbulence parameters were calculated from LDV measurements with the exception of the inlet velocity profile. All optical parameters were set and held constant throughout the series of measurements so as to insure continuity of technique and minimize sources of error. A net frequency shift of 10 MHZ $\pm$ 1 KHZ was employed throughout the series of measurements so as to eliminate the problem of incomplete signal bias. In addition, the sampling technique of Roesler, et al. [11] was employed to minimize velocity bias.

For each data point sampled the TSI processor output three digital numbers; n(exponent), D_m(digital mantiesa), N(cycles/burst). These three numbers were converted to a frequency, f_i, using the following equation:

$$f_i = \frac{N \times 10^9}{D_m \times 2^{n-2}} \tag{4}$$

Velocity was then determined using

$$V_i = (f_i - f_s)F_R \tag{5}$$

where f_s is the net frequency shift, f_i is the frequency determined from Equation (4) and F_R is the fringe spacing as derived in the Appendix.

The mean velocity, $(\bar{V})_\phi$ and variance $(\overline{v'^2})_\phi$ were found in Equations (6) and (7).

$$(\bar{V})_\phi = \frac{1}{m} \sum_{i=1}^{m} (V_i)_\phi \tag{6}$$

$$(\overline{v'^2})_\phi = \frac{1}{m} \sum_{i=1}^{m} [(V_i)_\phi - (\bar{V})_\phi]^2 \tag{7}$$

where m is the number of individual realizations and ϕ represents the angular orientation of the transmitting optics and thus the direction of the measured velocity component with respect to the horizontal. The values of ϕ used in this study were 0^o, 30^o, -30^o. Measurements more than three standard deviations from the mean were discarded as noise and $(\bar{V})_\phi$ and $(\overline{v'^2})_\phi$ were then recalculated using Equations (6) and (7). The number of points discarded was generally less than 20 from a total sample of 4500.

A method given by Logan [21,22] and described in detail by Bremmer, et al. [23] was then used to determine flow and turbulence parameters. Applying measurement at 0^o, $+30^o$ and -30^o yields:

$$\bar{U} = \frac{1}{m} \sum_{i=1}^{m} (V_i)_{\phi=0} = (\bar{V})_{\phi=0} \tag{8}$$

$$\bar{v}_\theta = (\bar{V})_{\phi=+30} - (\bar{V})_{\phi=-30} \tag{9}$$

$$(\overline{u'^2})^{1/2} = [(\overline{v'^2})_{\phi=0^o}]^{1/2} \tag{10}$$

$$(\overline{v_\theta'^2})^{1/2} = [2(\overline{v'^2})_{\phi=30} + 2(\overline{v'^2})_{\phi=-30} - 3(\overline{v'^2})_{\phi=0}]^{1/2} \tag{11}$$

$$\frac{1}{2}(\overline{u'^2} + \overline{v_\theta'^2}) = (\overline{V'^2})_{\phi=30} + (\overline{V'^2})_{\phi=-30} - (\overline{V'^2})_{\phi=0} \qquad (12)$$

$$\overline{u'v_\theta'} = [(\overline{V'^2})_{\phi=30} - (\overline{V'^2})_{\phi=-30}] \; / \; \sqrt{3} \qquad (13)$$

where $\overline{U}$ and $(\overline{u'^2})^{1/2}$ are the streamwise mean velocity and RMS velocity respectively and $\overline{v_\theta}$ and $(\overline{v_\theta'^2})^{1/2}$ are the circumferential mean velocity and RMS velocity respectively. All measurements were made on a horizontal diameter of the test section that was aligned with the optical axis.

The system geometry was axially symmetric, but it was not necessarily true that the flow downstream of the sudden expansion was axially symmetric. Thus it was necessary to determine if the symmetry condition existed for the flow downstream of the step. This was done by two means. As a coarse check static pressure measurements were taken circumferentially at three streamwise locations. These measurements showed no asymmetry in the flow. The second more sensitive technique involved taking LDV measurements across the full diameter of the test section at the $\phi=0^o$ angle only. The results showed that the mean flow and RMS velocities were indeed axially symmetric. Because of this, only measurements along one radius in the horizontal plane were required to map the flow field.

Measurements were first taken along the streamwise centerline of the cylindrical test section to obtain centerline velocity decay and the corresponding turbulence intensity behavior. The second set of measurements was made along four radial gridlines at planes downstream of the sudden expansion. There were nine streamwise measurement points and five angular measurement points per gridline with ten streamwise

points being spaced five mm apart and angular measurements ten mm apart. The experimental grid is shown in Figure 11. The Reynolds number for the axisymmetric sudden expansion based on step height and inlet centerline velocity was 3.59×10^4, which corresponds to an inlet centerline velocity, U_o=25.65m/s. The inlet conditions were that of a relatively flat inlet profile with a very low turbulence level (on the order of one percent).

2.2 Results

Centerline Parameters

One would expect that a similarity would exist between the centerline parameters for the flow just downstream of a step in a turbulent sudden expansion and the near field region of a free jet in that both flows have a core region in which the centerline velocity is maintained followed by a region of centerline velocity decay. From this point the similarity between the free jet and sudden expansion ceases to exist, since the free jet velocity decreases to zero while the sudden expansion flow decays to a flow characteristic of that for fully developed turbulent pipe flow. Figure 12 shows that these trends are exhibited by the data obtained in this study. Also shown in this figure is the corresponding data obtained by Moon and Rudinger [8] and Freeman [5]. The data obtained in the present study shows very good agreement with that of both Freeman [5] and Moon and Rudinger [8] when plotted as a function of downstream distance normalized with step height. This result is in spite of the fact that the ratio of step height to inlet radius is different (by as much as a factor of two) in the three cases and the inlet velocity pro-

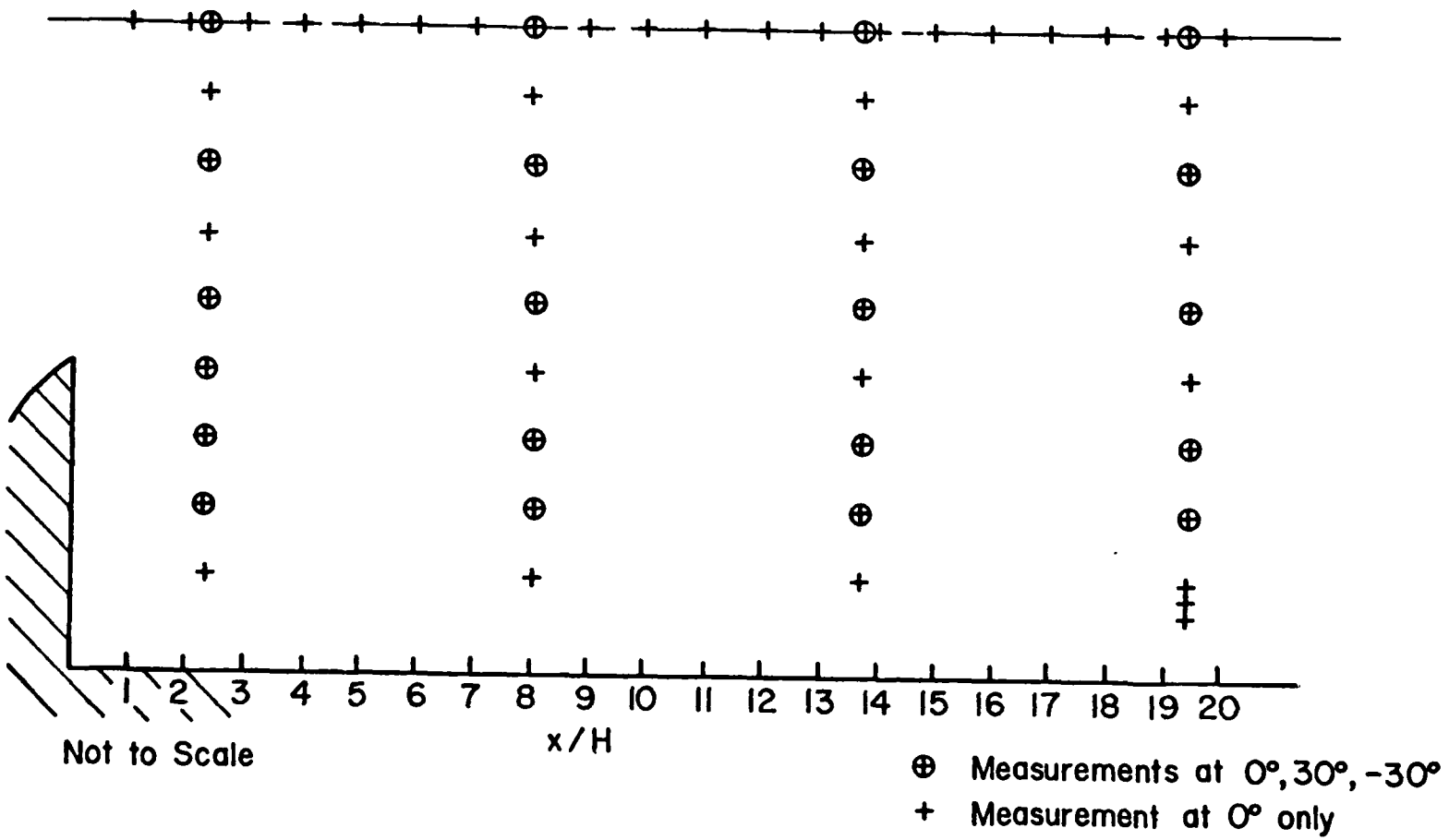

Figure 11 Experimental measurement grid

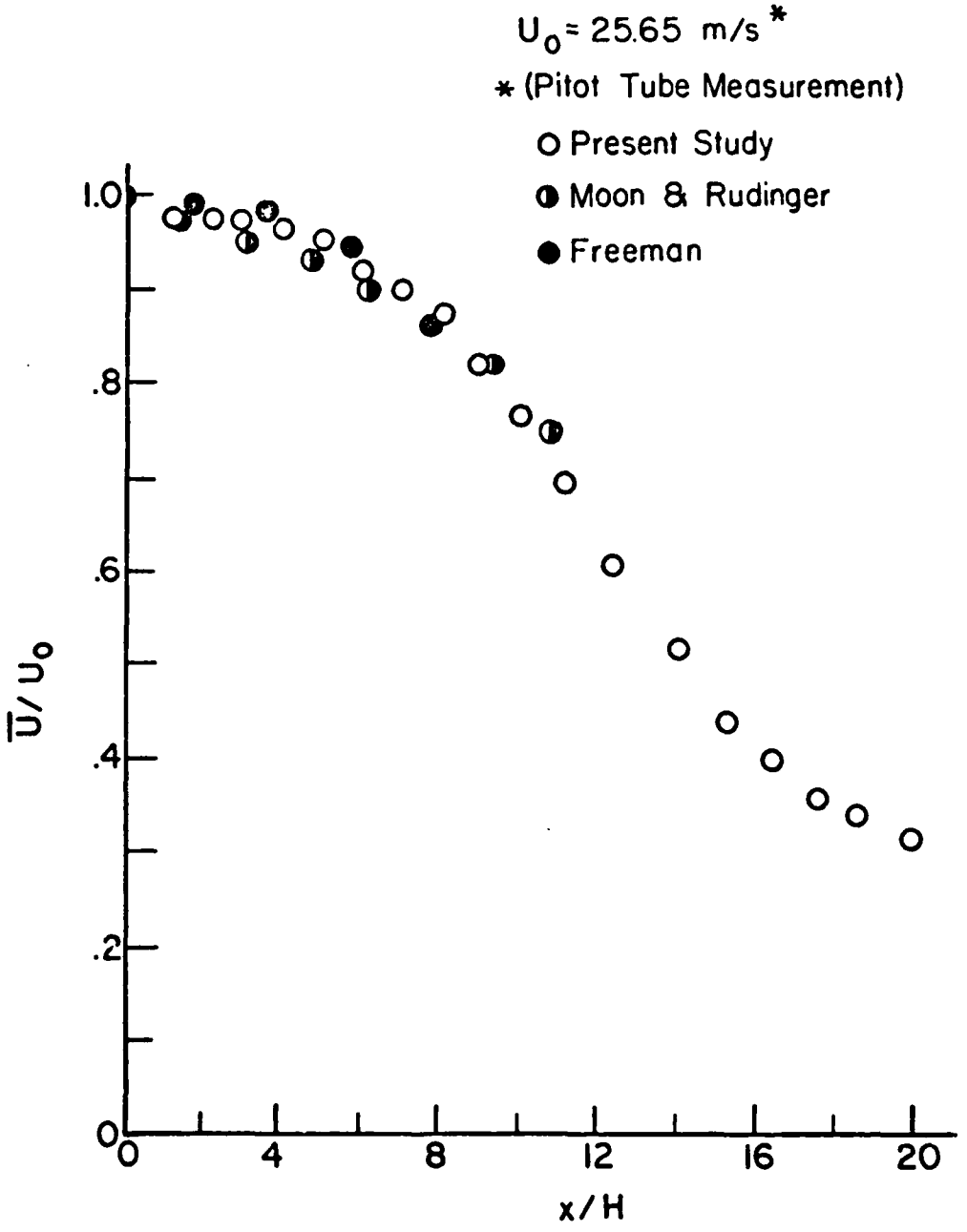

Figure 12 Mean centerline velocity decay

files also differ substantially. The discrepency in velocity ratio at the inlet between the observed velocity and 1.0 is probably due to the fact that the reference velocity in this study was measured with a pitot-static tube and all subsequent measurements were made using the LDV (LDV measurements could not be made exactly at the plane of the step due to the finite angle of the beams).

Figure 13 shows the turbulence intensity along the centerline. It can be seen that the turbulence intensity is quite low (~1.2%) at the inlet and then rapidly increases to a maximum at 13 step heights downstream. This maximum local value of turbulence intensity (38%) is much higher than one would expect as a centerline value and is of the same magnitude as that found in the near wall region of a fully developed pipe flow. This indicates that the flow in the center region of the pipe is much more interesting than one might expect. The method used for determination of turbulence intensity and all other statistical parameters can be found in the Appendix.

Streamwise Profiles

The mean and RMS streamwise velocities are both obtained from direct LDV measurements. Figure 14 shows the mean velocity profiles at the inlet, 2.29, 8.00, 13,71, and 19.43 step heights downstream of the step. The maximum recirculation velocity was approximately 10% of the centerline velocity at 2.29 step heights downstream. This value is in good agreement with the data obtained by both Freeman [5] and Moon and Rudinger [8]. It is also interesting to note the velocity profile at x/H=13.71 where the centerline turbulence intensity is approximately 38% (Figure 12). This profile is not indicative of having such a high turbulence level near

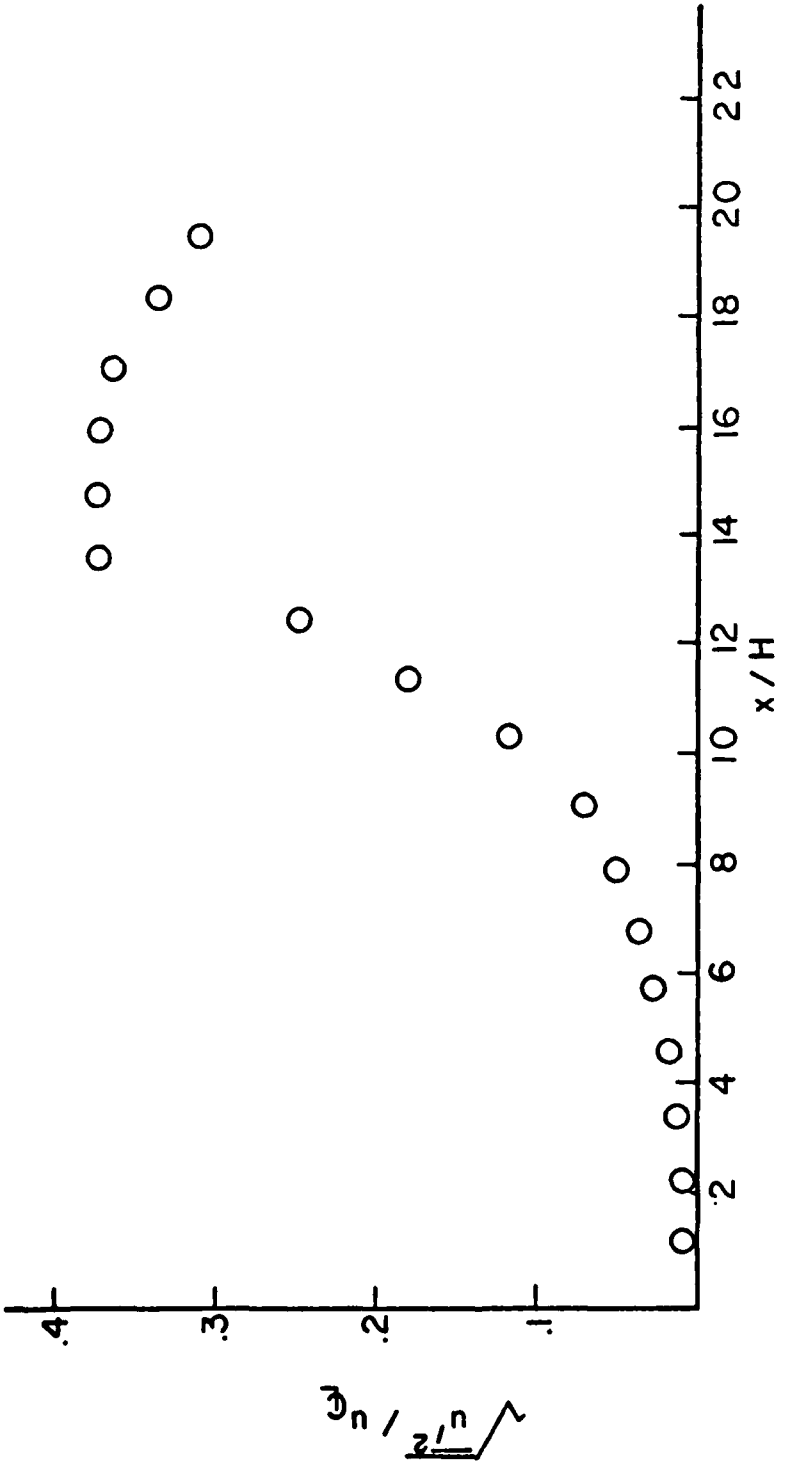

Figure 13 Centerline turbulence intensity profile (local values)

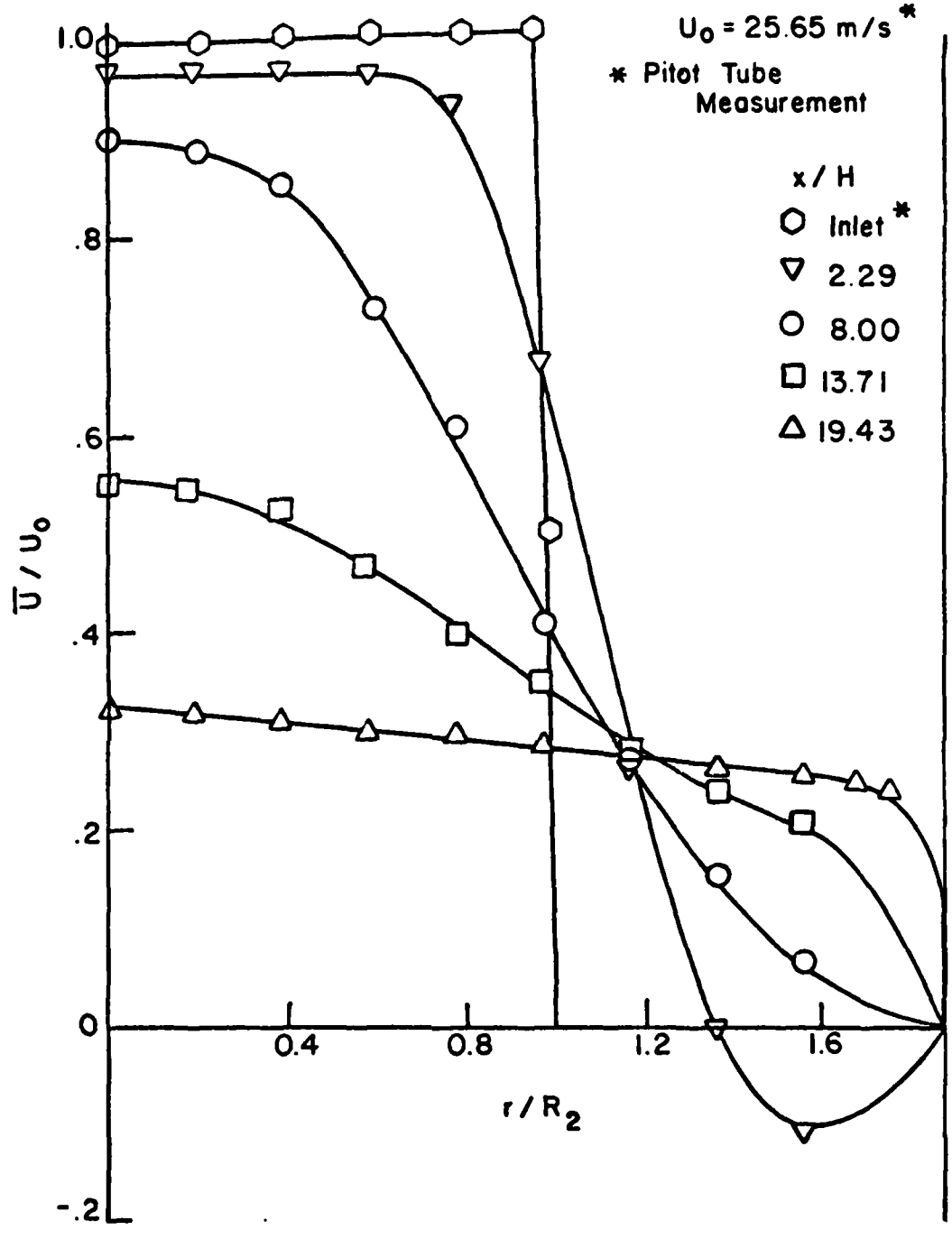

Figure 14 Measured mean streamwise velocity profiles

the centerline. This fact could possibly be interpreted as the flow having some mean field or shear layer oscillation since the histogram for this data point is somewhat skewed (S=.128).

As an accuracy check, the velocity profiles were used to calculate the massflow at each measurement plane. Figure 15 shows the non-dimensionalized integrated mass flow as a funciton of both radius and streamwise location. These results were obtained by integrating a polynomial fit of the data from Figure 14. Massflow is conserved at all of the gridlines to within 1% except for the data at x/H=19.43. It will be shown later that the probable reason for this was insufficient data near the wall. Since massflow as computed from the velocity profile data was conserved for the first three measurement grids the data obtained is considered accurate. This also indicates that velocity bias was eliminated by the data sampling method used. A more complete discussion of the massflow data is presented later in Section 4.

Figure 16 shows the measured turbulence intensity profiles. In the core region, very low values of turbulence intensity on the order 1.5 percent were measured. The maximum value (24 percent) of turbulence intensity was found in the recirculation region at x/H=2.29. Freeman, by comparison, found that the maximum turbulence intensity of 18 percent in his data occurred at x/H=4.0. As the shear layer spreads there is a decrease in the maximum turbulence intensity at any given plane. At x/H=19.43 the shear layer has all but dispersed and the turbulence intensity approaches a near uniform value across the test section. These results are in good overall agreement with those presented by Freeman. The data showed little scatter and the trends were as expected for this type of flow field.

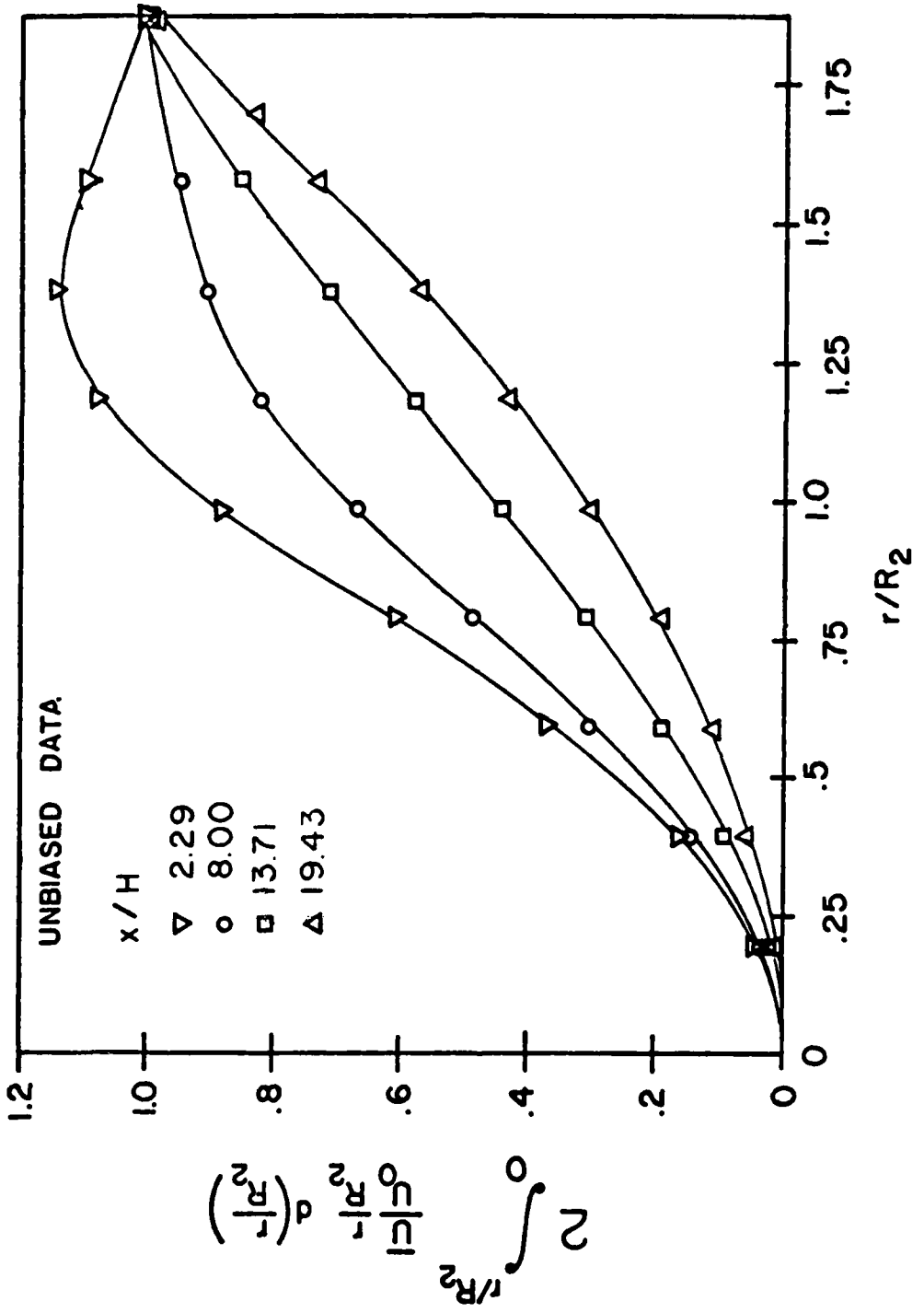

Figure 15 Integrated normalized mass flow rate

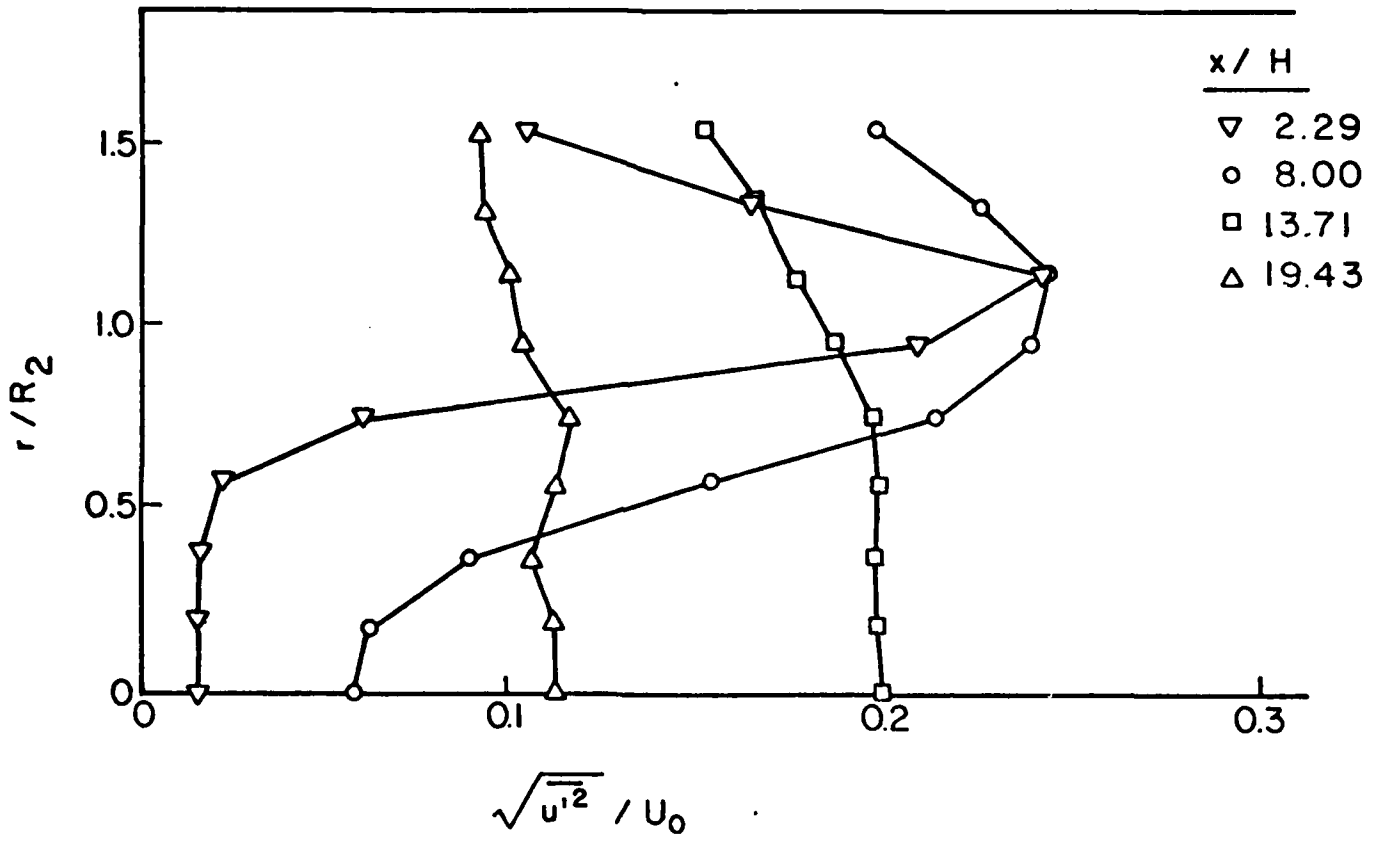

Figure 16 Measured streamwise turbulence intensity profiles

Flow Parameters Derived from Angular Measurements

Obtaining values for $\overline{v}_\theta(\overline{v_\theta'^2})^{1/2}$, $\overline{u'v_\theta'}$ and $(\overline{u'^2+v_\theta'^2})^{1/2}$ required the use of relations presented in Section 2.1 applied to the LDV measurements at 0^o, $+30^o$ and -30^o to the horizontal. Because of the indirect technique which involves subtracting measured values of similar magnitude, the accuracy will not be as good as that for the directly measured streamwise quantities. It should be noted that all θ parameters plotted on the centerline (r/R_2=0) are actually radial parameters.

Figure 17 shows the profiles for the mean circumferential velocity. At the x/H=2.29 gridline there appears to be very little circumferential motion in the core region, but there is a sizeable increase in this parameter as the shear layer is approached. The circumferential velocity reaches a maximum near the reattachment plane and then decreases at larger distances downstream. Since there is only a marginal circumferential velocity component at x/H=2.29, one could assume that very little swirl existed at the inlet to the sudden expansion and that the swirl was produced and maintained in the flow field. This result is similar to that found by Drewry [7].

Figure 18 shows the profiles obtained for the RMS circumferential velocity. The trends were as expected, that is, low circumferential turbulence levels in the core region, high turbulence in the recirculation zone and shear layer, and an approach to a uniform value across the tube as the flow reattaches and develops. Two items worth noting about this parameter are that the RMS value is roughly an order magnitude larger than the mean value and that the circumferential turbulence is of the same order as the streamwise values.

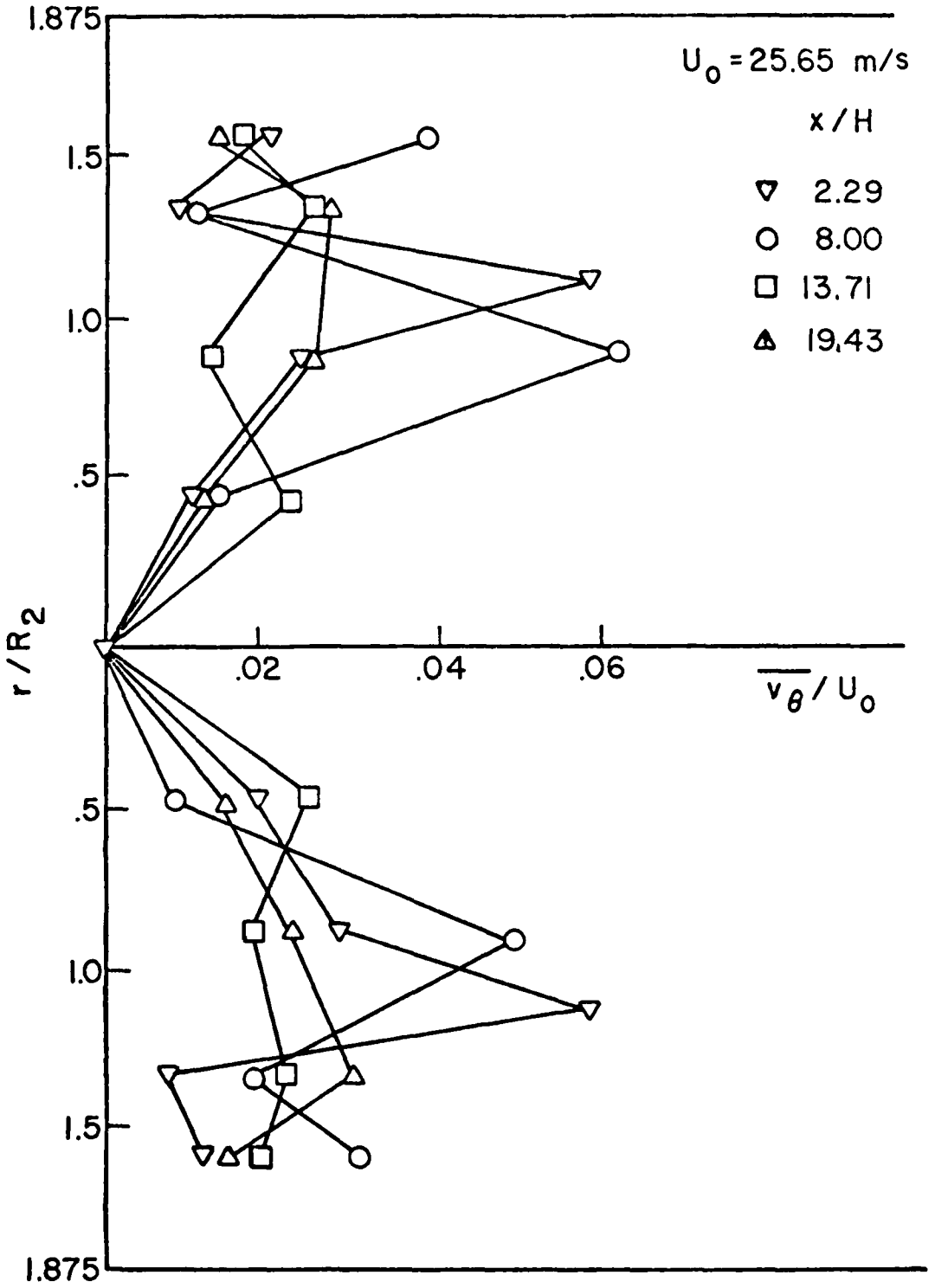

Figure 17 Measured mean circumferential velocity profiles

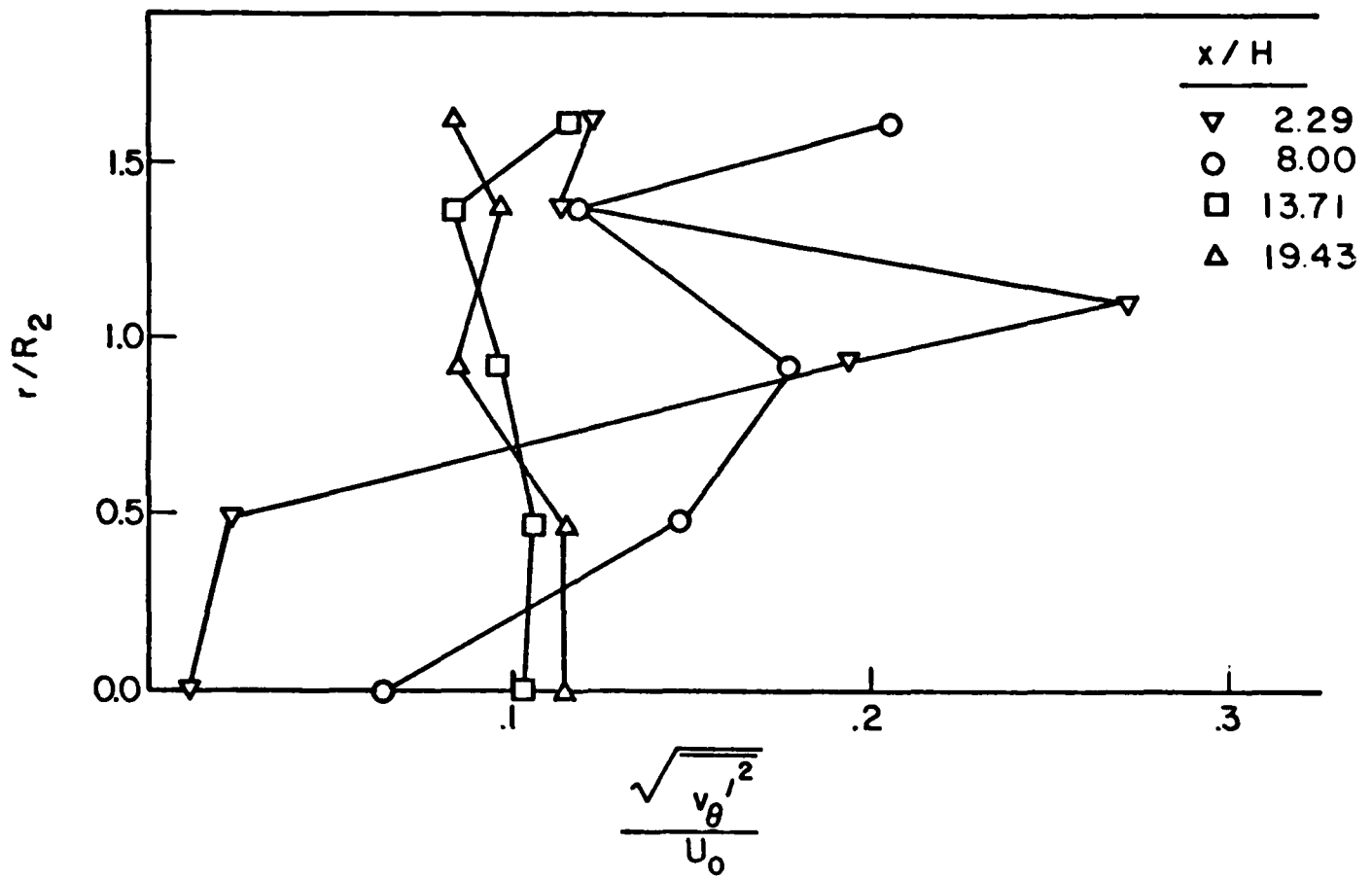

Figure 18 Measured circumferential turbulence intensity profiles

Reynolds stress profiles are shown in Figure 19. The plot shows that these turbulence stresses reach their maximum in the region near reattachment and decay to lower values as the flow becomes more developed. As to the magnitude of the measured stresses, the values are small (generally less than an order of magnitude smaller) when compared to the axial-radial Reynolds stress for fully developed pipe flow. This tends to show that the axial-circumferential Reynolds stress is rather insignificant in this flow although the data shows some interesting trends. It is worth noting that at x/H=2.29 and x/H=8.00 where a peak or valley occurs in the measured Reynolds stress there is a corresponding peak or valley in both the mean and RMS value of circumferential velocity. Also where the Reynolds stress becomes more well behaved (x/H=13.71 and x/H=19.43) $\bar{v}_\theta$ and $\overline{v_\theta'^2}$ also become well behaved.

Figure 20 shows the profiles of turbulent kinetic energy based on the circumferential RMS veloctiy. In the core region where turbulence levels are low, the turbulent kinetic energy is correspondingly low. The recirculation zone and the region near reattachment have the highest levels of turbulent kinetic energy. As the flow develops, the turbulent kinetic energy levels out approaching a near uniform value at 19.43 step heights downstream of the step. Although there appears to be some disorder in this parameter, it may not all be totally unexpected. The reasoning behind this is that one expects the total turbulent kinetic energy to have only one inflection, but this is the sum of all three RMS component velocities squared. One also expects one inflection for profiles of $\overline{u'^2}$, $\overline{v_\theta'^2}$ and $\overline{v_r'^2}$ but by no means does this impose that the sum of any two have only one inflection. Thus some of the disorder in

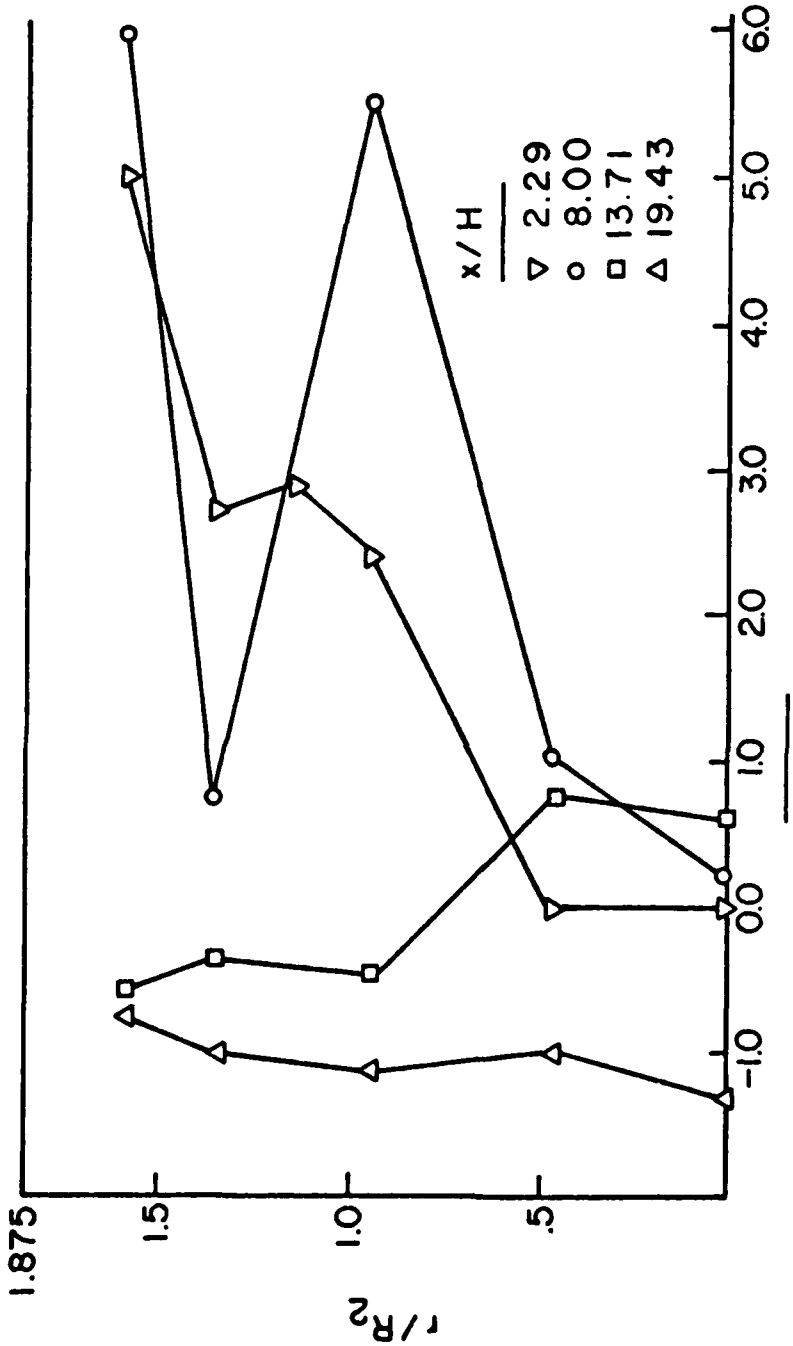

Figure 19 Normalized measured Reynolds stress

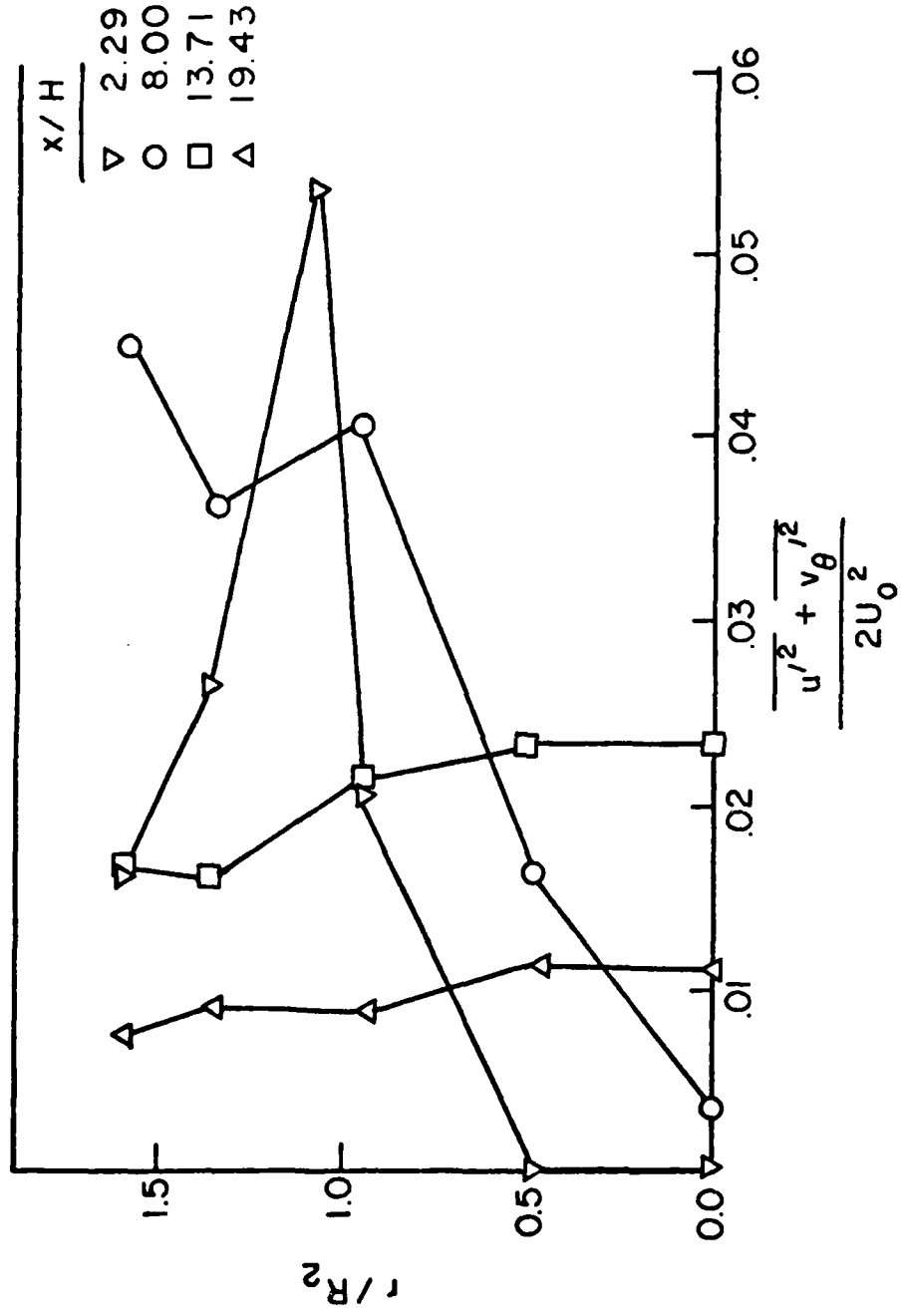

Figure 20 Normalized measured turbulent kinetic energy profiles

Figure 20 may be due to measurement error but some may also be expected. Lastly it was noted that this value for turbulent kinetic energy follows the same trends with $\overline{v}_\theta$ and $\overline{v}_\theta'^2$ as the Reynolds stress did.

3. Reattachment length

Reattachment length was determined by obtaining values of stream function numerically from the mean streamwise velocity data. The stream function is defined by

$$\overline{U} = \frac{\partial \psi}{\partial r} \tag{14}$$

Using second order central differencing about the points i and i+1, equation (15) can be approximated by

$$\frac{\overline{U}_{i+1} + \overline{U}_i}{2} = \frac{\psi_{i+1} - \psi_i}{r_{i+1} - r_i} + f(x) \tag{15}$$

At any given x-plane f(x) will be a constant and can be arbitrarily set to zero. Because of this, equation (15) becomes

$$\psi_{i+1} = \psi_i + (r_{i+1} - r_i)\left(\frac{\overline{U}_{i+1} + \overline{U}_i}{2}\right) \tag{16}$$

The stream function values, calculated from equation (16), were then tabulated and contours of stream function were determined for specific values of this parameter. The results are shown in Figure 21. From these results the reattachment length was found to be 7.93 step heights (x/R_2=6.94). This value is in good agreement with earlier results reported in the literature [3, 5, 7, 8, 23].

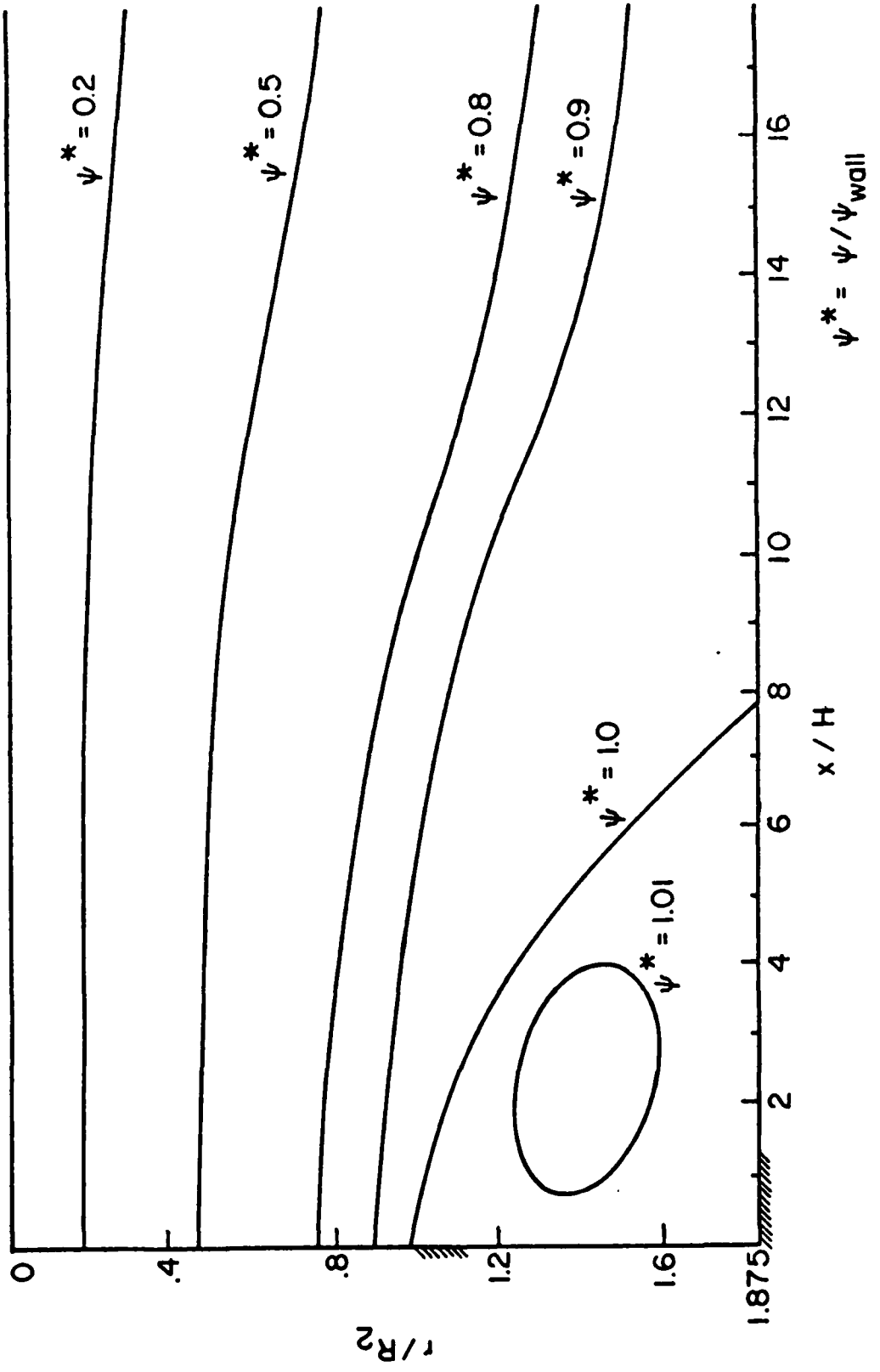

Figure 21 Normalized stream function contours

4. Massflow Rate

4.1 Measurements

In this study two sets of measurements were taken at the $\phi=0^{o}$ angle only. One set of measurements, considered to be unbiased, was taken with particle arrival rates in excess of 20,000 Hz and a computer sampling rate of 25 samples per second. The second set of data was taken with a particle arrival rate of 5000 Hz and free sampling, that is, the microcomputer was allowed to sample data as fast as it could. The mean velocity data were then reduced and integrated using piecewise integration with forward polynomial fitting to the data points and backward direct integration of the polynomial fit. The experimental grid in this study employed the same four gridlines as those stated previously for X/H=2.29, 8.00, and 13.71. For X/H=19.43 grid points were spaced 5 mm apart up to 40 mm off the centerline with extra grid points at 42 and 43 mm to permit definition of the thin boundary layer at this location. Measurements at these extra grid points were achieved using a specially machined circular tube which had a 1/8 inch wall thickness from X/H=0 to X/H=18.28 and a wall thickness of 1/16 inch from X/H=18.28 to X/H=20.57. This thin wall section reduced aberation effects and allowed the probe volume to be located closer to the tube wall.

4.2 Results

Figures 22-25 show integrated massflow as a function of radius at the four measuring stations. Figure 22 clearly shows the characteristics of a recirculation zone. In this figure it should be noted that integration of velocity data obtained without concern for velocity bias leads

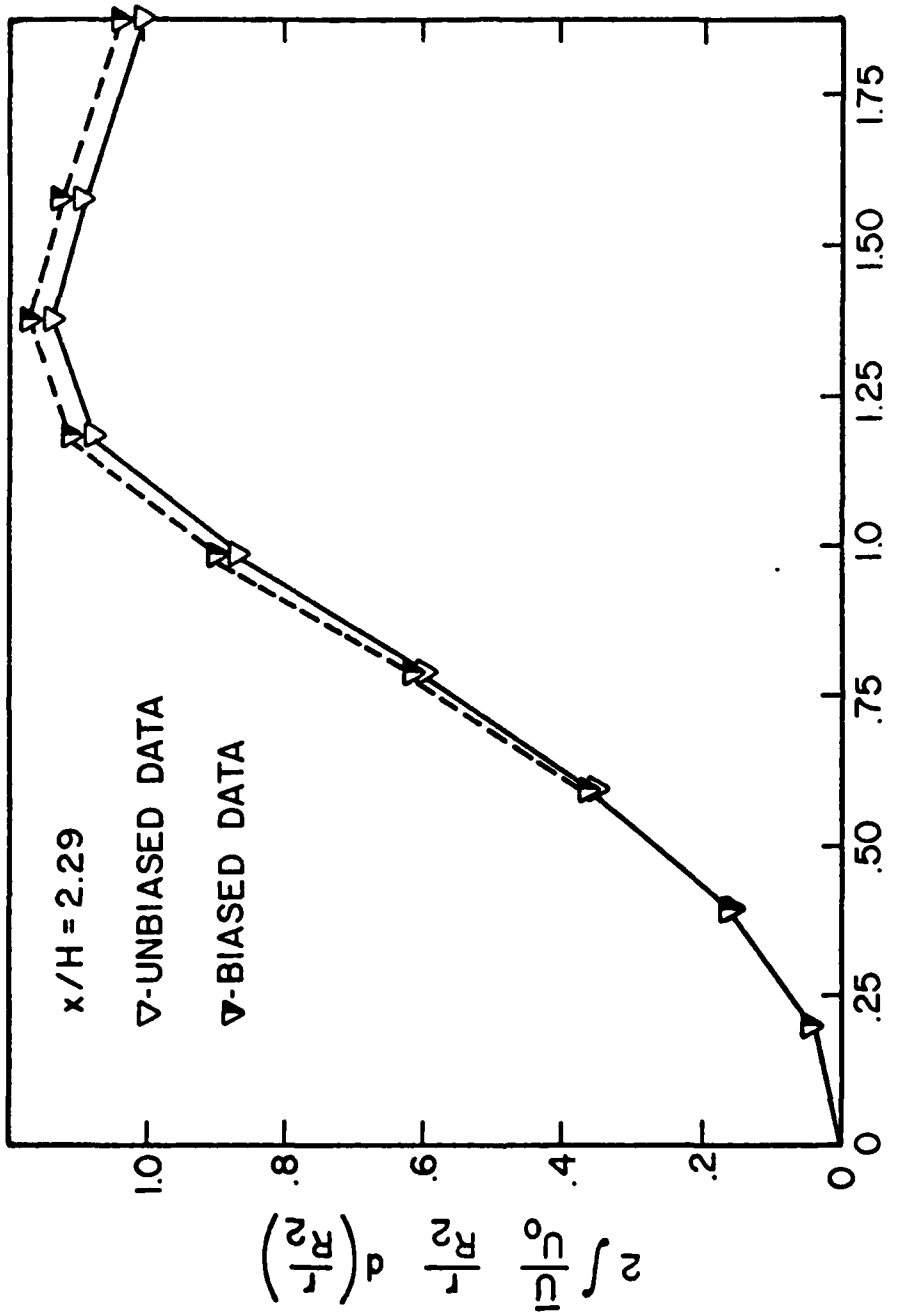

Figure 22 Comparison of biased to unbiased mass flow rate at x/h=2.29

to approximately a three percent difference in massflux compared to the unbiased data. It is apparent that in the core region where turbulence levels are low there is virtually no difference in the massflux obtained using either data sampling technique, but as the turbulence level increases so does the amount of velocity bias. At this particular gridline (x/H= 2.29) the massflux error caused by velocity bias is somewhat compensated for by the resulting higher recirculation velocities.

In Figures 23 and 24 the problem of velocity bias becomes much more pronounced. Here errors reach a maximum of six percent. This occurs because of the high turbulence levels in this region and lack of recirculation velocities to compensate for those in the mean flow direction. At x/H =8 velocity bias becomes visible earlier than at x/H=13.71 because the flow is highly turbulent near the reattachment point and the amount of bias is related to the turbulence level whereas at x/H=13.71 the flow is beginning to develop and is not quite so turbulent. As to the validity of the polynomial fitting procedure near the wall at x/H=13.71, the data were also integrated using a 1/4 power law fit between the last data point and the wall. The difference in massflow between the two fitting procedures was small (approximately 1%). Therefore the procedure used initially is believed to be accurate at this x location.

Figure 25 shows the integrated massflow at 19.43 step heights downstream of the step. At this location the flow is essentially that of a developing turbulent pipe flow. To obtain the data necessary for an accurate integration at this grid line the special test section described previously was used. This test section allowed measurements to be taken to within 4.625 mm of the tube wall. Although it appears that the biased

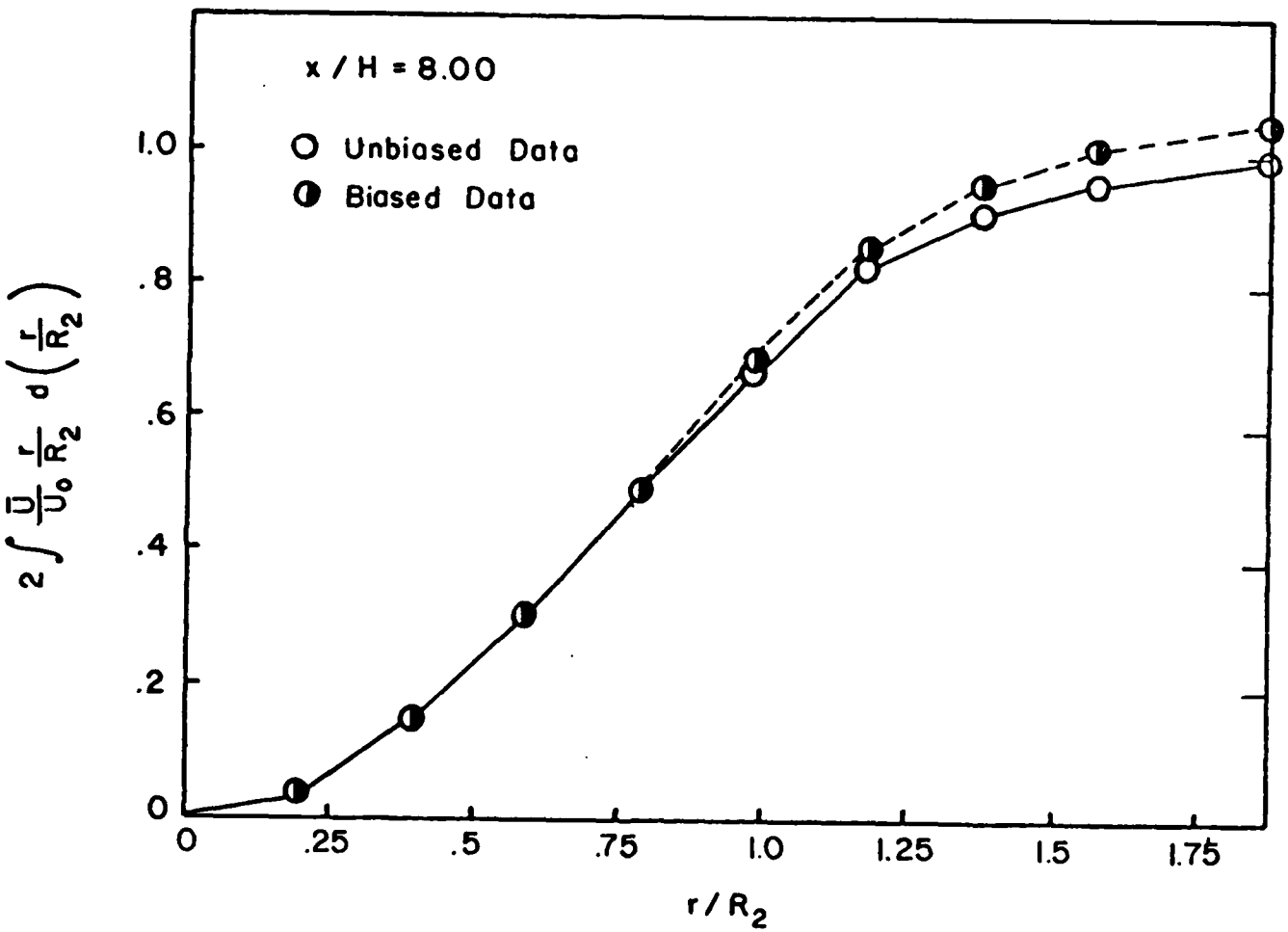

Figure 23 Comparison of biased to unbiased mass flow rate at x/H=8.00

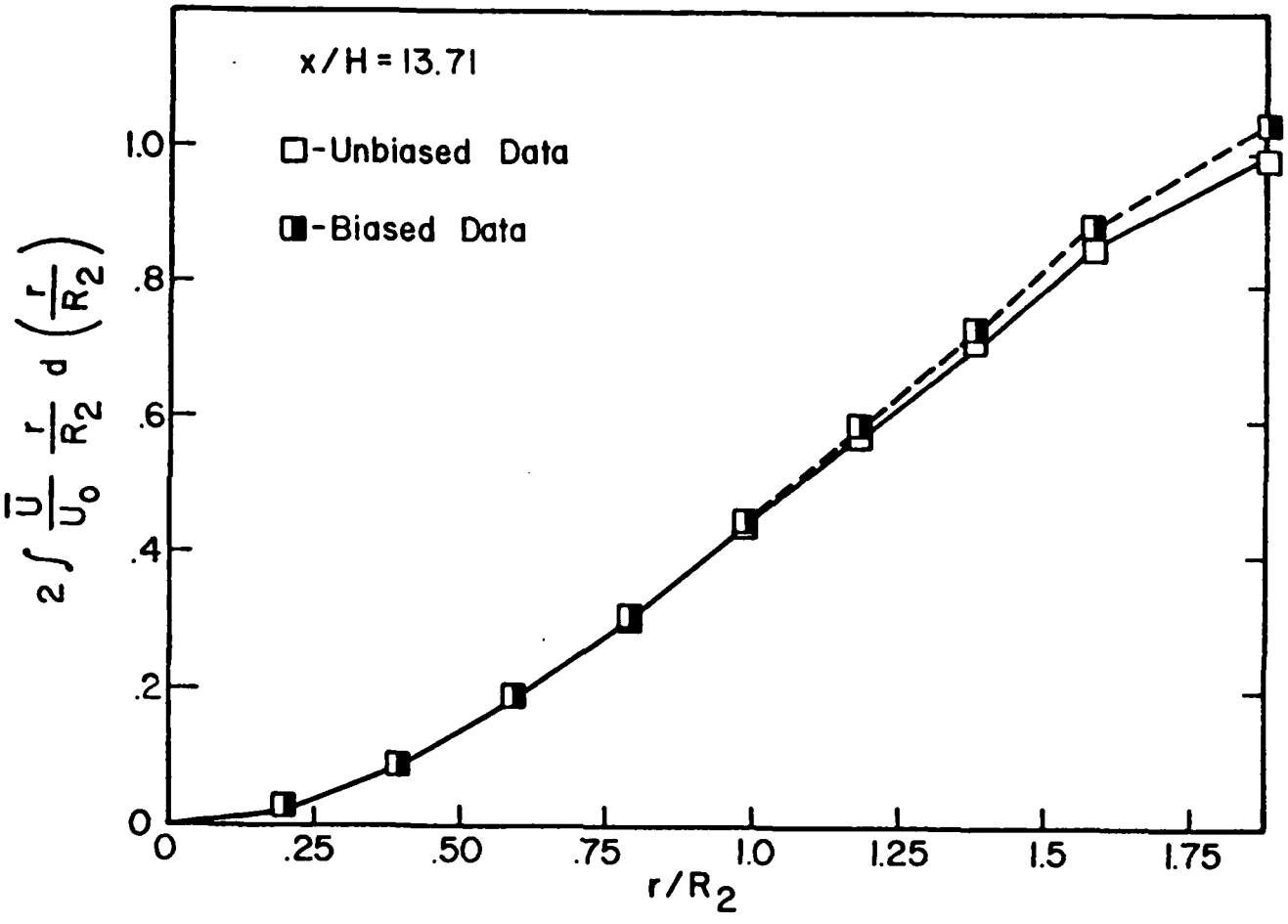

Figure 24 Comparison of biased to unbiased mass flow rate at x/H=13.71

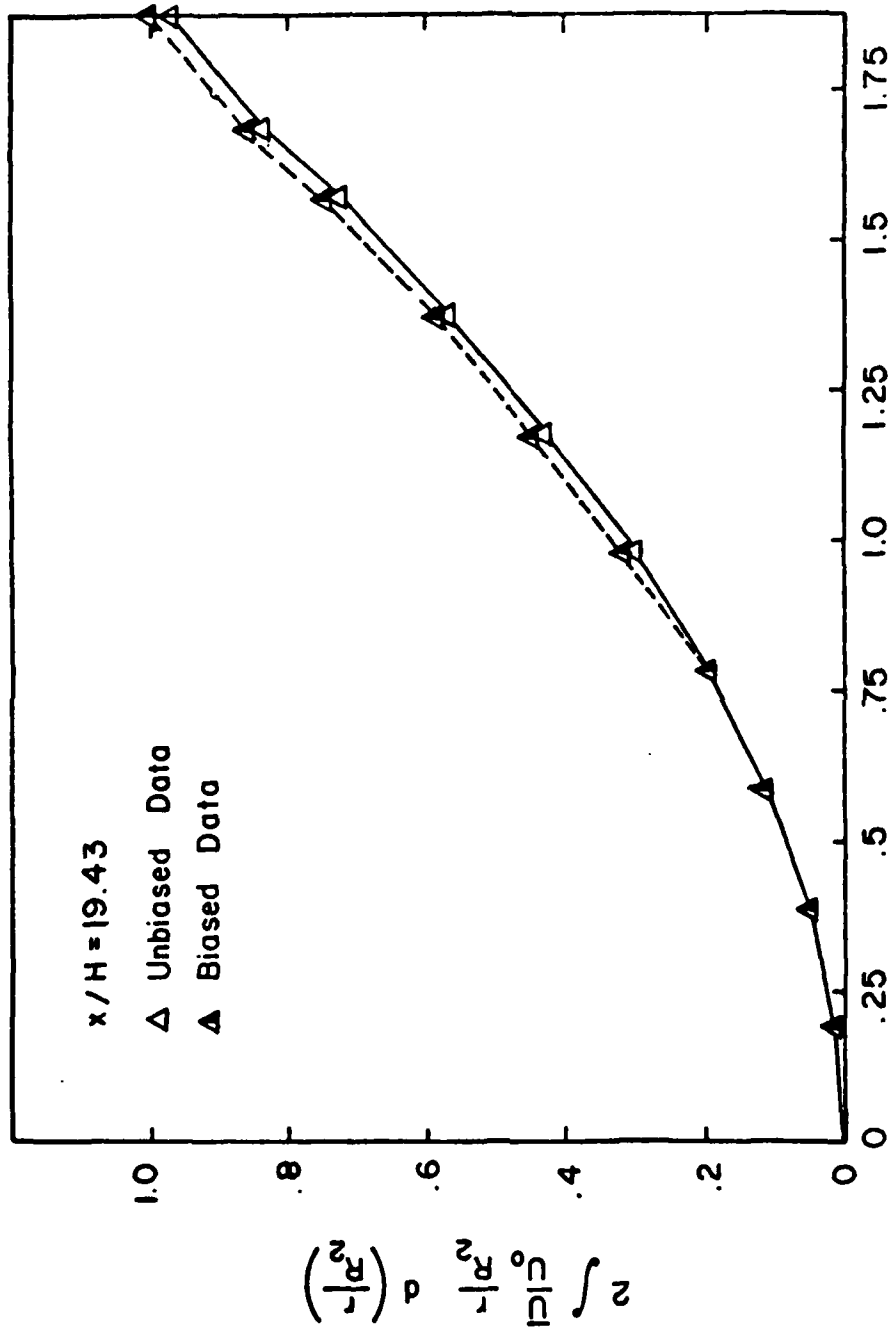

Figure 25 Comparison of biased to unbiased mass flow rate at x/H=19.43

data integrated to a more accurate value of massflow than the unbiased data at this plane using the polynomial fit, direct integration procedure described earlier, the last data point obtainable was still more than 4 mm from the wall which is in the region where the velocity gradient is substantial. Therefore a substantial amount of massflow could have been missed due to the incomplete definition of the true velocity profile near the wall. Using a power law fit between the last data point and the wall at this x location yielded a net increase in massflow of approximately 3.2%. Using this type of profile, for the biased data gave a total massflow over 3% greater than that of the inlet. Using the power law profile with the unbiased data showed a total massflow of 1% greater than the inlet massflow at this x location. Since the flow is turbulent at this x location, it should be expected that the flow should follow a power law profile rather than a 2nd degree polynomial (laminar) profile near the wall. It was also noted that the integrated value of massflow changed very little using the power law fit for exponents greater than 1/10 and less than 1/6. In any case the difference in massflux based on the unbiased data was less than 2.5 percent at x/H=19.43 as compared to the other stations.

5. Effect of Particle Velocity on Doppler Signal Amplitude

The measurements reported by Durão and Whitelaw [17] indicated that Doppler signal amplitude decreased with Doppler frequency (particle velocity). If true, this would tend to compensate for velocity bias due to the lower probability of detection by the processor. However, the existence of this effect has been questioned. Therefore a study of the dependence of signal amplitude on velocity was undertaken.

The study required permanent storage of Doppler signal amplitude. The data were taken along the centerline of the two-dimensional nozzle described in Section III. Data rates were in excess of 20,000 HZ and data was sampled at 25 HZ. The maximum signal amplitude was observed from photographs of individual Doppler bursts on the oscilloscope.

Figure 26 shows the results of this study. It can be seen that as the velocity, V, in the two-dimensional nozzle increases the Doppler signal amplitude essentially remains constant. There is some deviation in the maximum voltage from data point to data point due to the resolution of the photographs from which these values were obtained. Nevertheless the data are certainly adequate to show any significant trend. Obviously there was no observable decrease in signal amplitude with velocity over a range of nearly 6:1 (5.33-28.25m/s) which covers a major fraction of the velocities measured in the sudden expansion flow field. Therefore, at least in this study, no compensation of velocity bias by a velocity dependent signal amplitude was present. In fact the data in Figure 26 cast doubt on the reality of such a phenomenon.

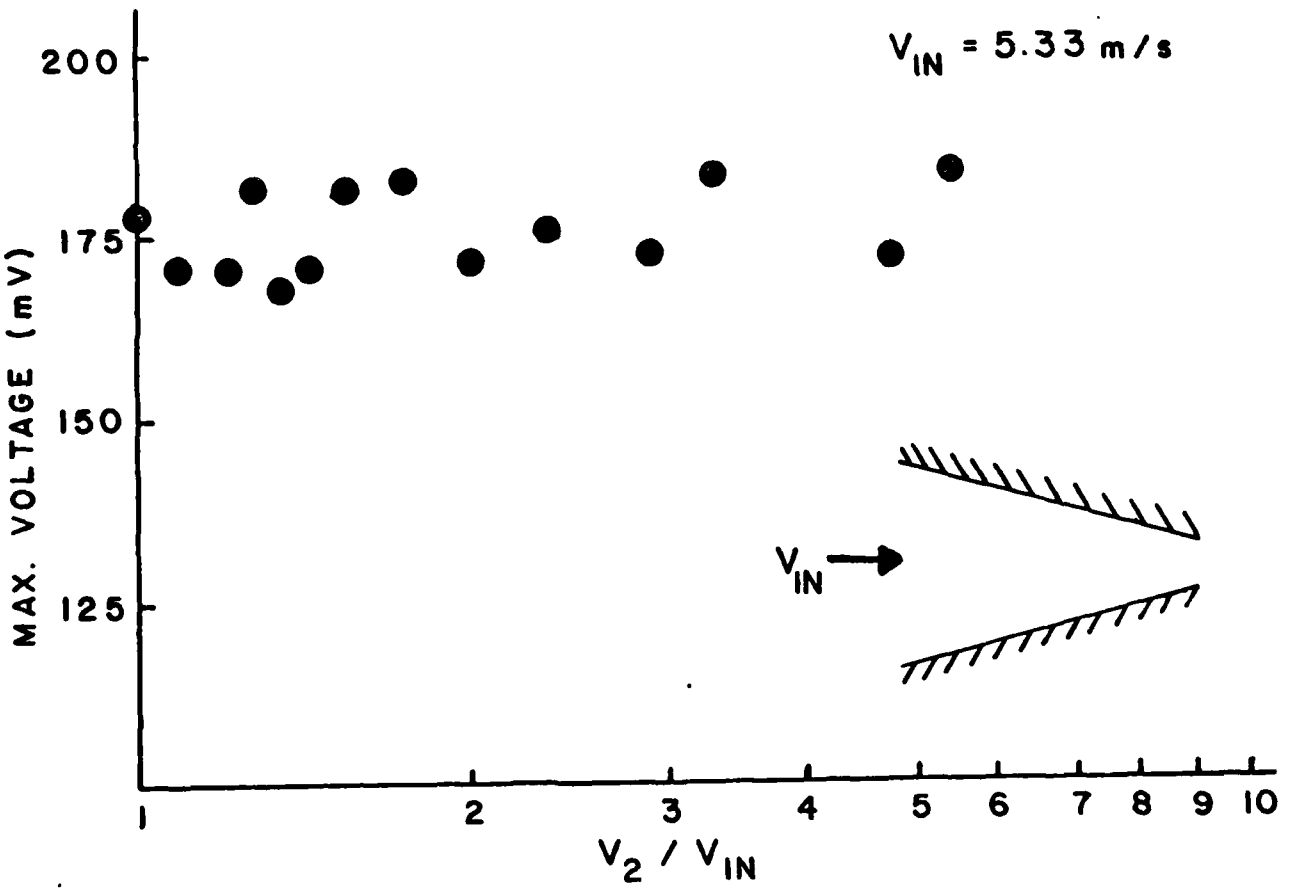

Figure 26. Maximum signal amplitude variation with velocity

SECTION V

COMPARISON OF NUMERICAL ANALYSIS WITH EXPERIMENTAL RESULTS

1. Introduction

In order to provide a basis for comparison of analytically predicted and measured flow parameters, the computer code CHAMPION 2/E/FIX of Pun and Spalding [24] was adapted to the flow geometry and run. This code uses the k-ε turbulence model of Launder and Spalding [25] along with a modified version of the SIMPLE algorithm described by Pantankar and Spalding [26].

The 2/E/FIX code, when adapted for an axisymmetric geometry, solves the partial differential equation

$$\frac{\partial}{\partial x}(\rho\bar{u}\phi) + \frac{1}{r}\frac{\partial}{\partial r}(\rho r\bar{v}_r\phi) = s_\phi + \frac{\partial}{\partial x}(\Gamma_\phi \frac{\partial\phi}{\partial x}) + \frac{1}{r}\frac{\partial}{\partial r}(\Gamma_\phi r\frac{\partial\phi}{\partial r}) \quad (17)$$

where r is the coordinate in the radial direction, x is the coordinate in the streamwise direction, $\bar{u}$ is the mean velocity in the streamwise direction, $\bar{v}_r$ is the mean velocity in the radial direction, ϕ is the dependent variable, Γ_ϕ is the exchange coefficient and s_ϕ is the source term. Equation (17) represents the time averaged Navier-Stokes equations along with a supplemental transport equation. The k-ε model assumes isotropic diffusion with the effective viscosity, μ_{eff}, being the sum of the laminar and turbulent contributions.

When appropriate expressions for ϕ, s_ϕ and Γ_ϕ as listed in Table 1 are substituted into the general Equation(17), the equation takes on the form of continuity, axial and radial momentum, turbulent kinetic energy and rate of energy dissipation equations.

Table 1. Conservation expressions corresponding to Equation 17 .

Conservation of	ϕ	Γ_ϕ	S_ϕ
Mass	1	0	0
Axial momentum	$\bar{u}$	μ_{eff}	$\frac{\partial}{\partial x}(\mu_{eff}\frac{\partial \bar{u}}{\partial x})+\frac{1}{r}\frac{\partial}{\partial r}(\mu_{eff}\, r\frac{\partial v_r}{\partial x})-\frac{\partial p}{\partial x}$
Radial momentum	$\bar{v}_r$	μ_{eff}	$\frac{\partial}{\partial x}(\mu_{eff}\frac{\partial \bar{v}_r}{\partial x})+\frac{1}{r}\frac{\partial}{\partial r}(\mu_{eff}\, r\frac{\partial \bar{v}_r}{\partial r})$
Turbulent kinetic energy	k	μ_{eff}/σ_k	$G_k - \rho\varepsilon$
Turbulent energy dissipation	ε	$\mu_{eff}/\sigma_\varepsilon$	$\frac{\varepsilon}{k}(C_1 G_k - C_2\rho\varepsilon)$

$$G_k = \mu_t\left[2\left[\left(\frac{\partial \bar{u}}{\partial x}\right)^2+\left(\frac{\partial \bar{v}_r}{\partial r}\right)^2+\frac{v_r^2}{r^2}\right]+\left(\frac{\partial \bar{u}}{\partial r}+\frac{\partial \bar{v}}{\partial r}\right)^2\right]$$

The 2/E/FIX code solves this set of simultaneous differential equations, with appropriate boundary conditions, using upwind differencing. The matrix equation obtained from the numerical approximations is then solved using a tridiagonal algorithm along with under relaxation to achieve numerical stability.

Inputs to the code include inlet velocity and turbulent kinetic energy profiles, grid locations, relaxation factors and five constants

used in the expressions listed in Table 1. The numerical values of these five constants recommended by Launder and Spalding [25] are given in Table 2. Although the constant C_D is in none of the expressions in Table 1, it is used in the following two equations

$$\mu_{turb} = C_D \rho k^2/\varepsilon \tag{18}$$

$$\bar{U} C_D^{1/4} k^{1/2}/(\tau_w/\rho) = \frac{1}{\kappa} \ln(E C_p^{1/4} k^{1/2} y_1 \rho/\mu_{lam}) \tag{19}$$

Equation 18 is the equation from which the turbulent contribution to viscosity is evaluated. Equation 19 represents a modified "log law" used to link the first node from the wall to the wall boundary condition where κ is a constant equal to 0.4, E is a constant equal to 9.0 for smooth walls, τ_w is the wall shear stress, $\bar{U}$ is the mean axial velocity at point y_1 and y_1 is the distance from the wall to the first node from the wall.

Table 2. Recommended turbulence constants from Reference 25

Constant	Value
C_D	0.09
C_1	1.43
C_2	1.92
σ_k	1.00
σ_ε	1.30

The grid size used in all computational runs was a 21 x 21 grid. This grid size was chosen because it leads to shorter run times than larger grids and yet gives results comparable to those obtained with larger grids as shown by Bremmer, et al. [23]. The channel length chosen for the analytic solutions was 20 inlet radii. This was done to make the exit boundary condition (no axial velocity gradients and no radial velocity) as valid as possible while maintaining a small Δx to keep numerical error small. The convergence criterion, built into the code, on $\bar{U}$, $\bar{v}_r$, turbulent kinetic energy (TKE) and turbulent energy dissipation (TED) was 10^{-3}.

2. Numerical Results

Reattachment length was chosen as a common flow field parameter for comparison of the numerical analysis to experimental results. Moon and Rudinger matched their experimental results in terms of reattachment length by setting the coefficients C_1=1.43 and C_2=1.70. In the present study only C_2 was iterated upon to match the experimental value of reattachment length. The data is shown in Figure 27. A least square linear fit was then applied to the data, yielding the following equation.

$$C_2 = -0.06785(x_r/H) + 2.48271 \qquad (20)$$

where x_r is the reattachment length and H is the step height. Since the observed reattachment length was approximately 7.9 step heights a value of 1.94 was chosen for C_2 based on this equation. This differs only slightly from the value of 1.92 suggested by Pun and Spalding.

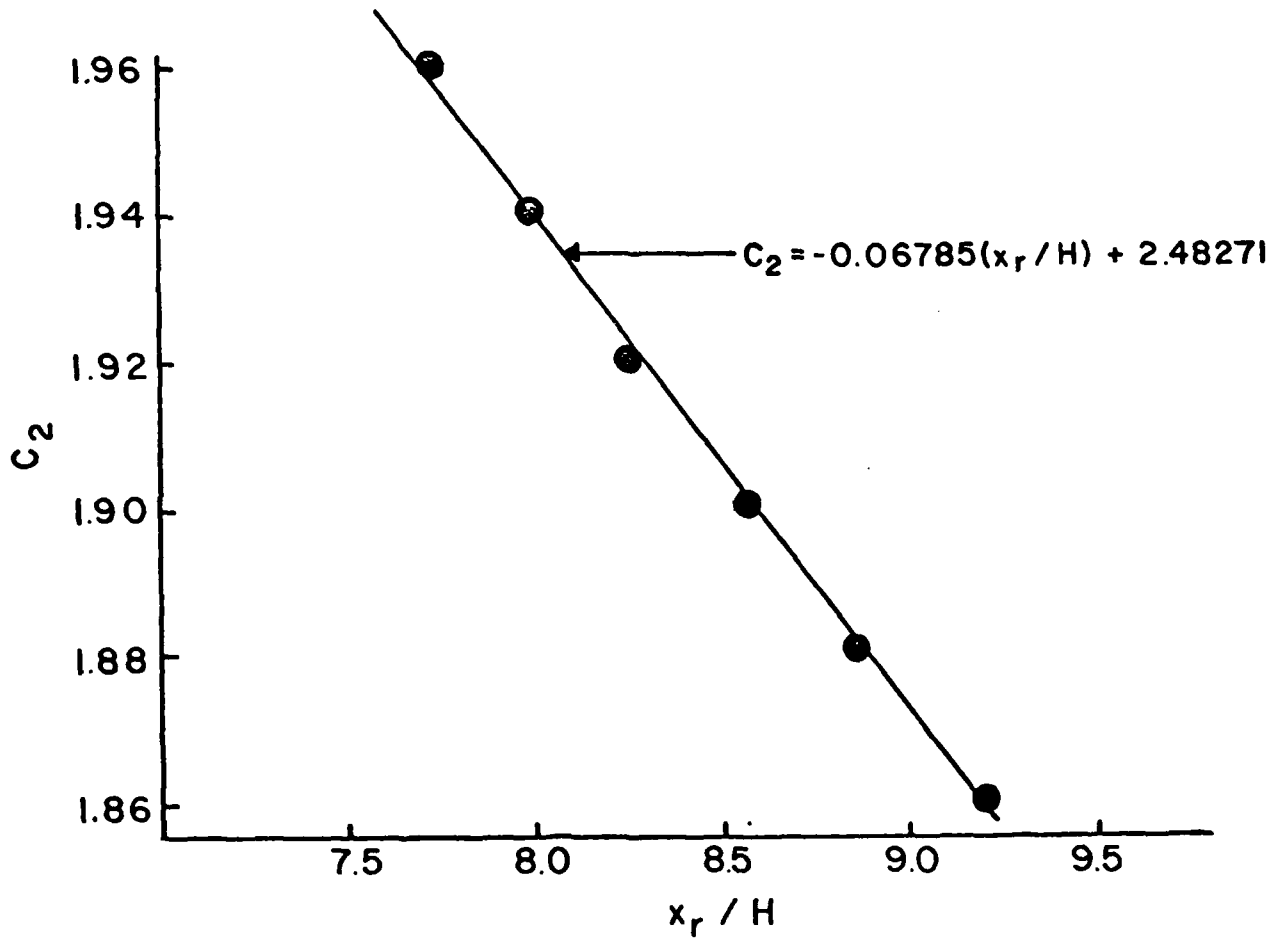

Figure 27 Turbulent dissipation rate coefficient variation with reattachment length

2.1 Mean Streamwise Velocity

Figure 28 shows a comparison of the computed and measured mean streamwise velocity on the centerline. As indicated by the figure, the numerical analysis predicts a more rapid decay in centerline velocity than the experimental results up to the point of reattachment. From this point the reverse is true and in the end a substantially higher mean streamwise velocity is predicted over that which was measured. One possible explanation for this occurrence is that the numerical analysis assumes a downstream exit boundary condition of no streamwise velocity gradients when in fact the experiment shows that this is not the case.

Figures 29 through 32 show velocity profile comparisons at different streamwise locations. At 2.29 step heights downstream of the step, as shown in Figure 29, the numerical prediction gives good agreement with the data obtained experimentally although there is a sizeable discrepency in the recirculation zone. The code predicts recirculation velocities much greater in magnitude than those found experimentally. Although the last grid point where this difference occurs is closer to the wall in the numerical analysis than the last measured data point, there is no reason to expect this higher recirculation velocity actually existed since massflow was checked in the experiment.

At reattachment, Figure 30, the velocity profiles are in reasonable agreement except near the centerline where the effect of the difference in centerline velocity decay noted earlier in Figure 28 is evident.

Once the flow reattaches and begins to develop, the numerical analysis produces an inflection in the predicted velocity profiles. This can be seen in the vicinity of $r/R_2 \cong 1.3$ in Figures 31 and 32. The velocity

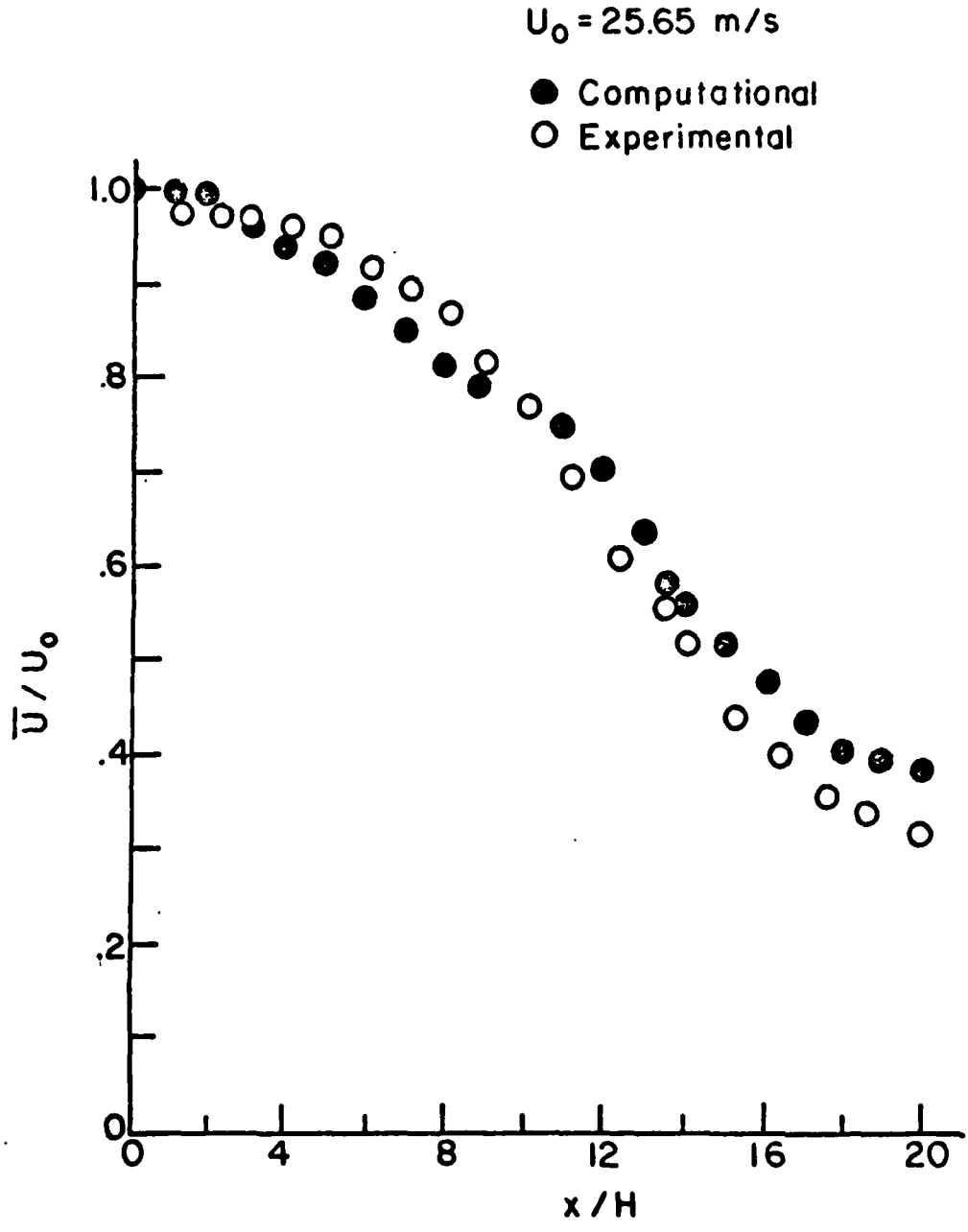

Figure 28 Comparison of predicted and measured centerline velocity decay

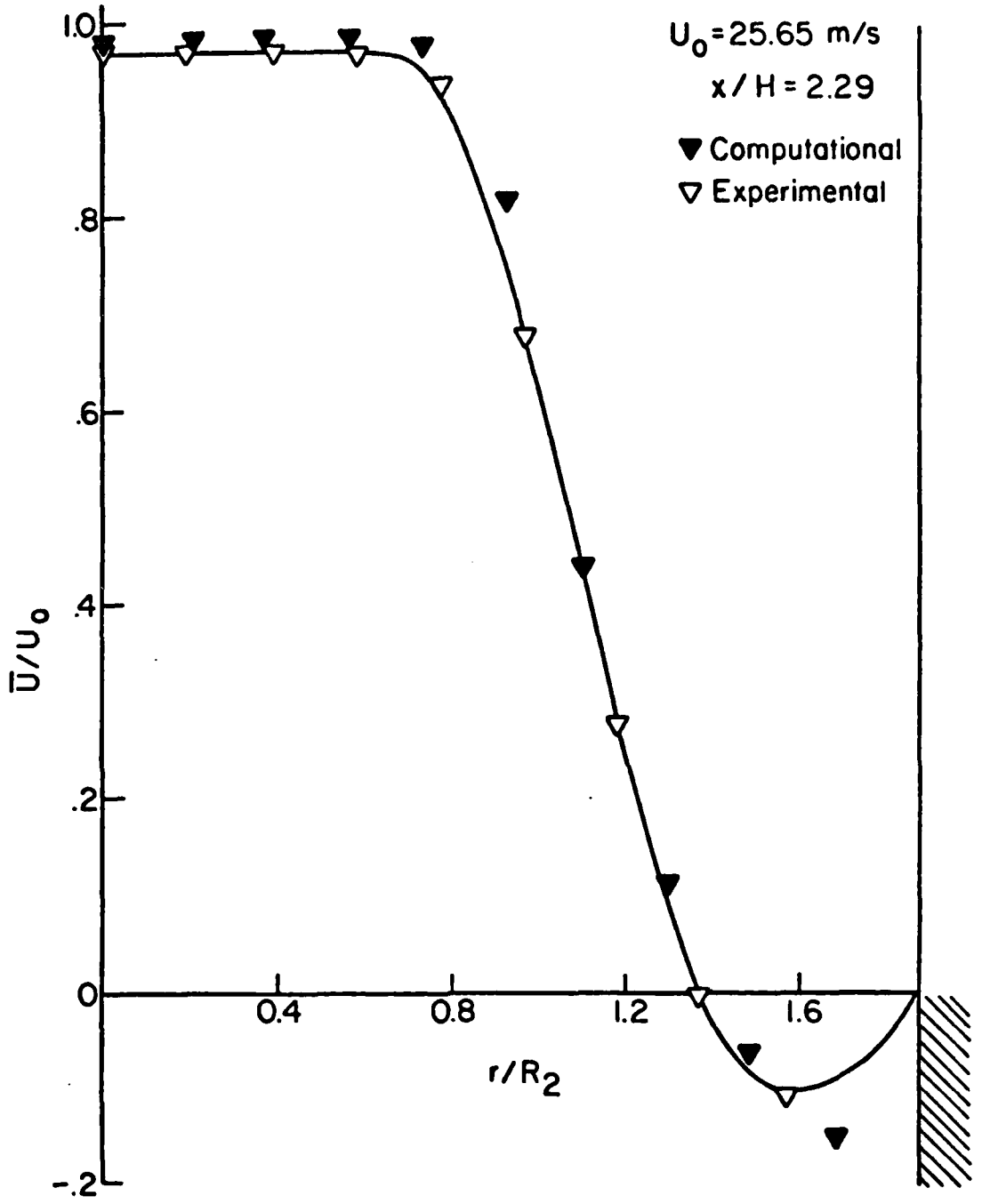

Figure 29 Comparison of predicted and measured mean streamwise velocity profile at x/H=2.29

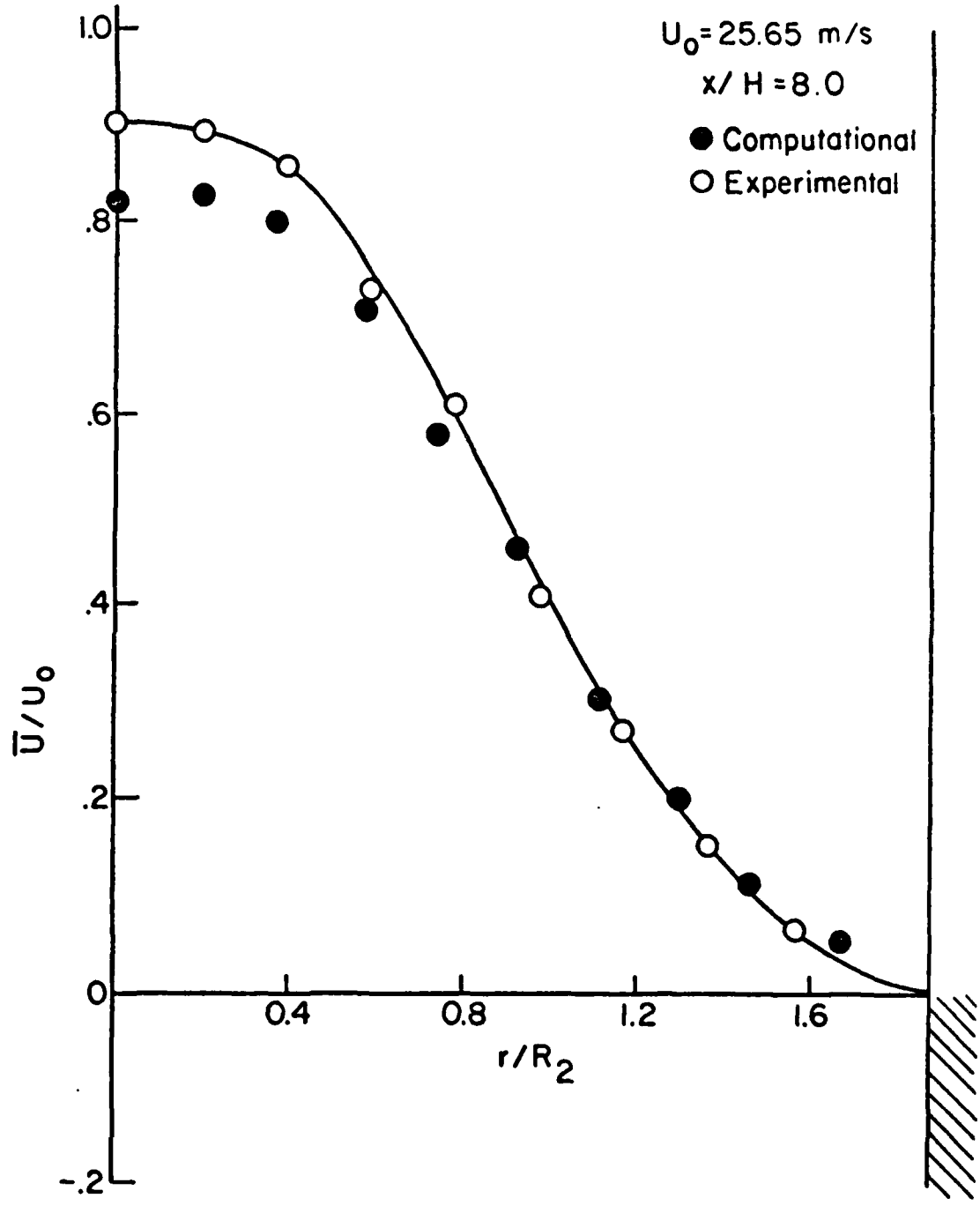

Figure 30 Comparison of predicted and measured mean streamwise velocity profile at x/H=8.0

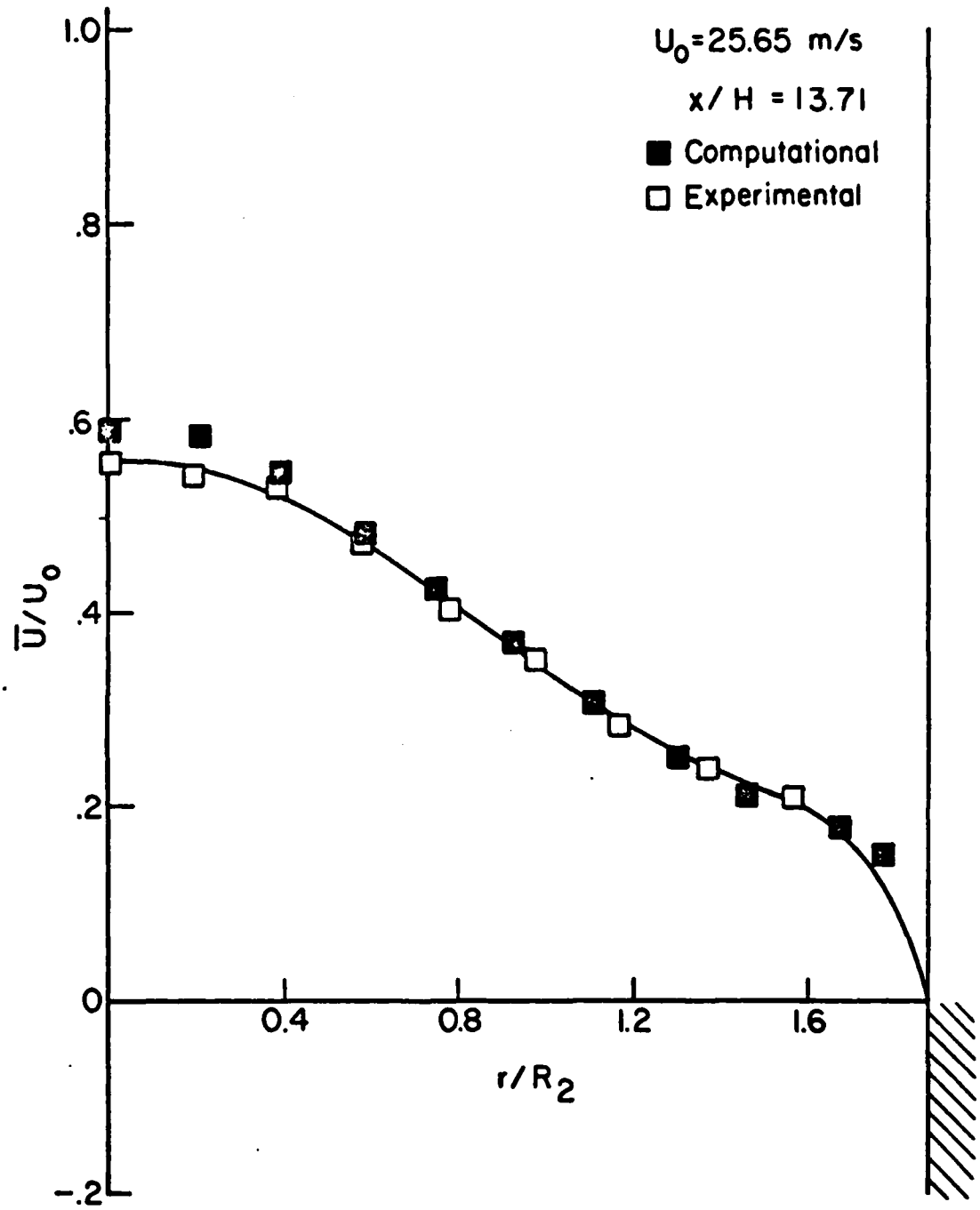

Figure 31 Comparison of predicted and measured mean streamwise velocity profile at x/H=13.71

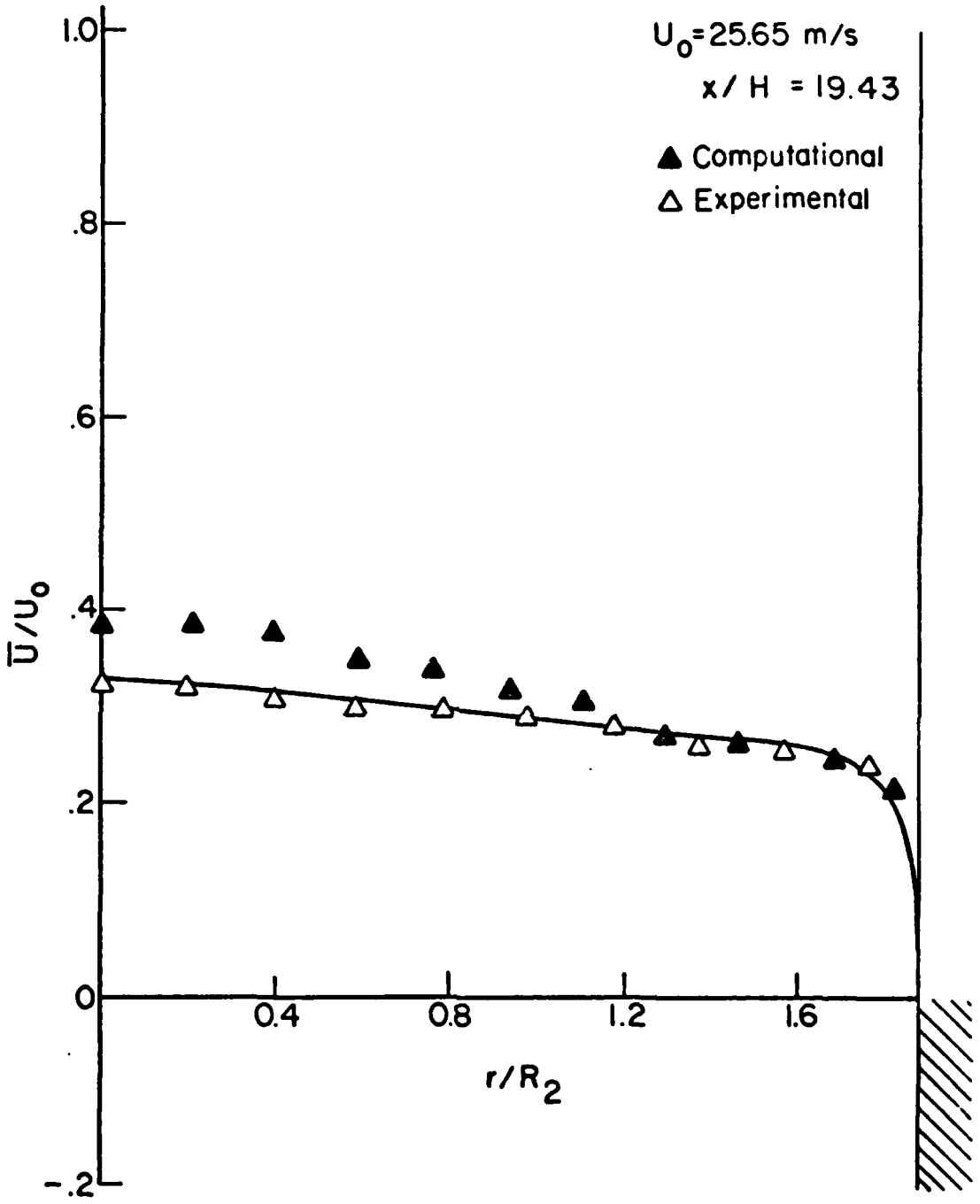

Figure 32 Comparison of predicted and measured mean streamwise velocity profile at x/H=19.43

profiles at x/H=13.71 (Figure 31) show very good agreement between theory and experiment. As the flow develops the profiles begin to deviate more. At x/H=19.43 (Figure 32) there is a large difference in velocity at the centerline of the test section. Although there is a large difference in velocity here, the difference in massflow rate is small since the flow area in this region is small (less than 30% of the total). Bremmer, et al. [23] also found increasing deviations in the more developed regions of the flow when using the same code adapted to a two-dimensional step geometry. An interesting note to recognize from Figures 29 through 32 is that, knowing mass has been conserved experimentally, there is no possible way that the computer code conserves mass. The massflow rate actually fluctuates from gridline to gridline and was found to be greater than that of the inlet in some cases and less than the inlet in others.

2.2 Turbulent Kinetic Energy

In the comparison of turbulent kinetic energy profiles, Figures 33 through 36, trends exhibited by the numerical analysis are correct although quantitatively low in all cases. One assumption made in this comparison was that since $\overline{v_\theta'^2}$ was the same order of magnitude as $\overline{u'^2}$, $\overline{v_\theta'^2}$ should be the same order as $\overline{v_r'^2}$. This was a necessary assumption since the computer code based the turbulent kinetic energy on $\overline{v_r'^2}$. In any event the predicted values of turbulent kinetic energy were lower than those experimentally measured in opposition to the results obtained by Bremmer, et al. [23] in the two-dimensional study. As a matter of interest it was found that changing the inlet turbulent kinetic energy in the program by a factor of five had only a marginal effect on the TKE values downstream and no effect on the mean velocity field.

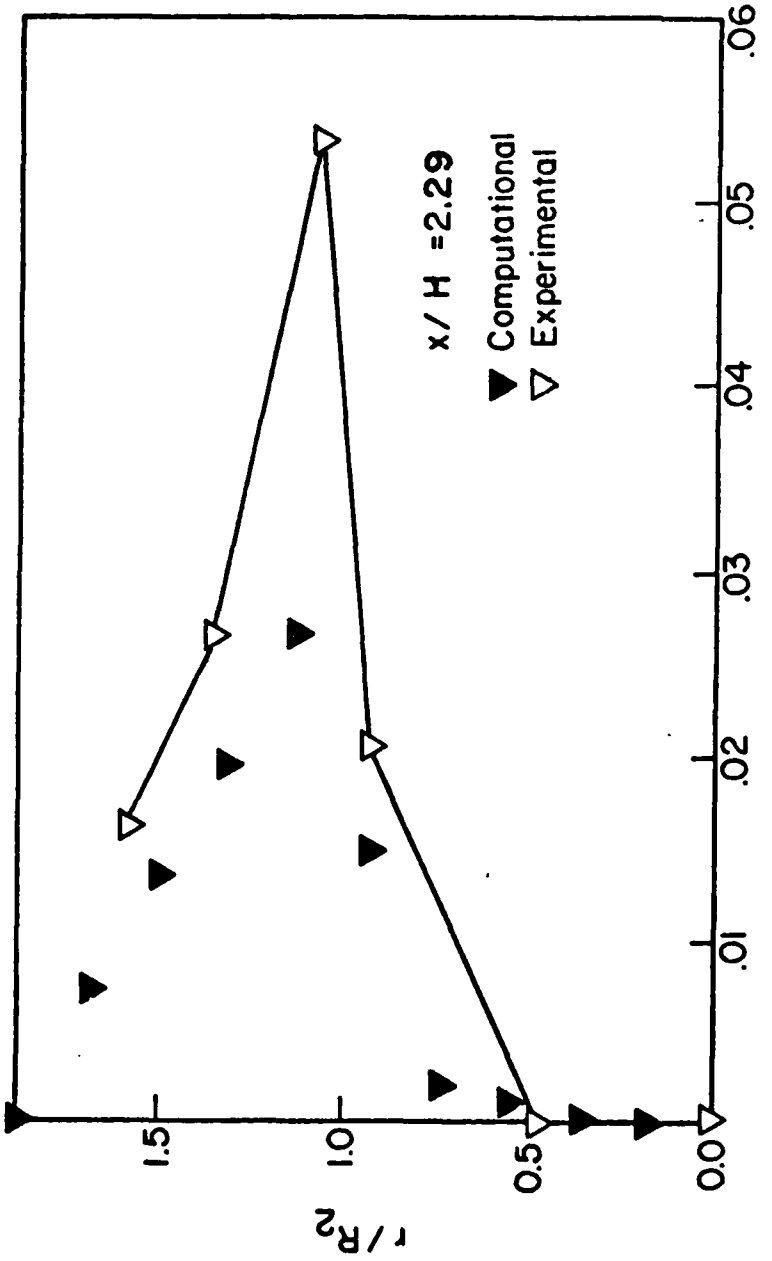

Figure 33 Comparison of predicted and measured turbulent kinetic energy at x/H=2.29

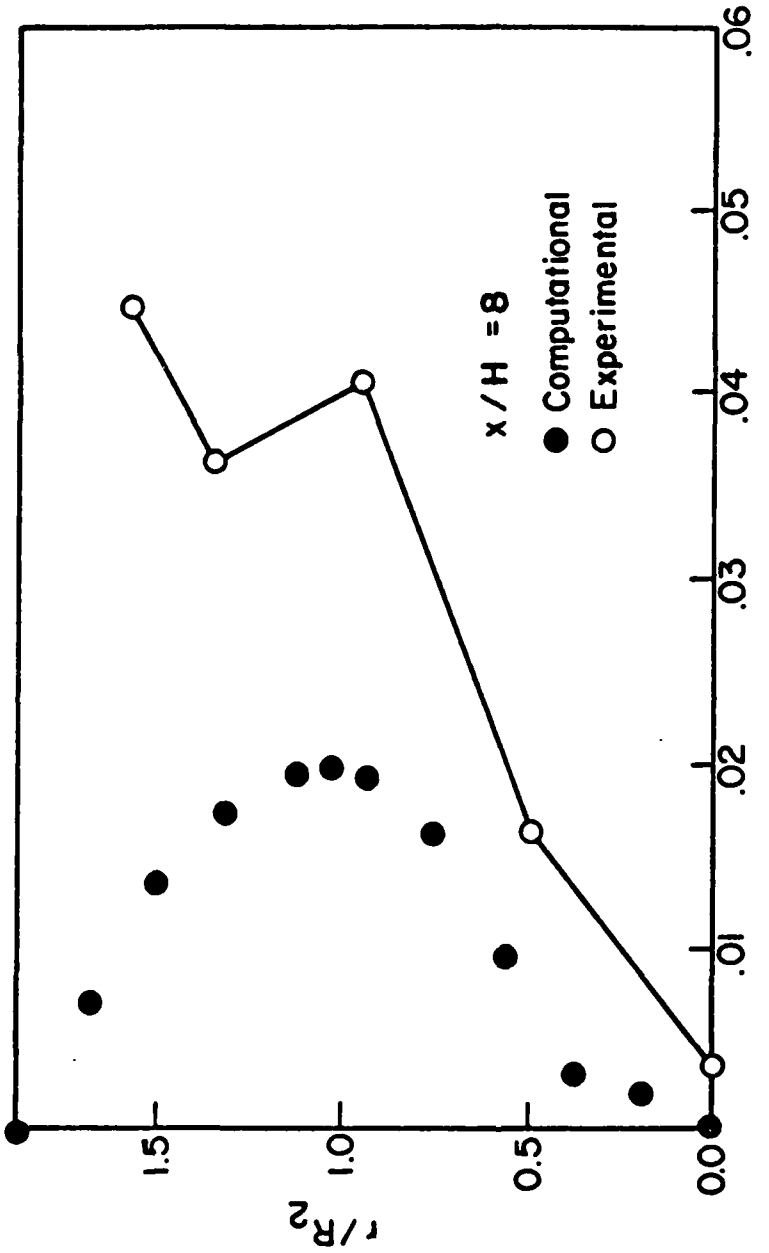

Figure 34 Comparison of predicted and measured turbulent kinetic energy at x/H=8.00

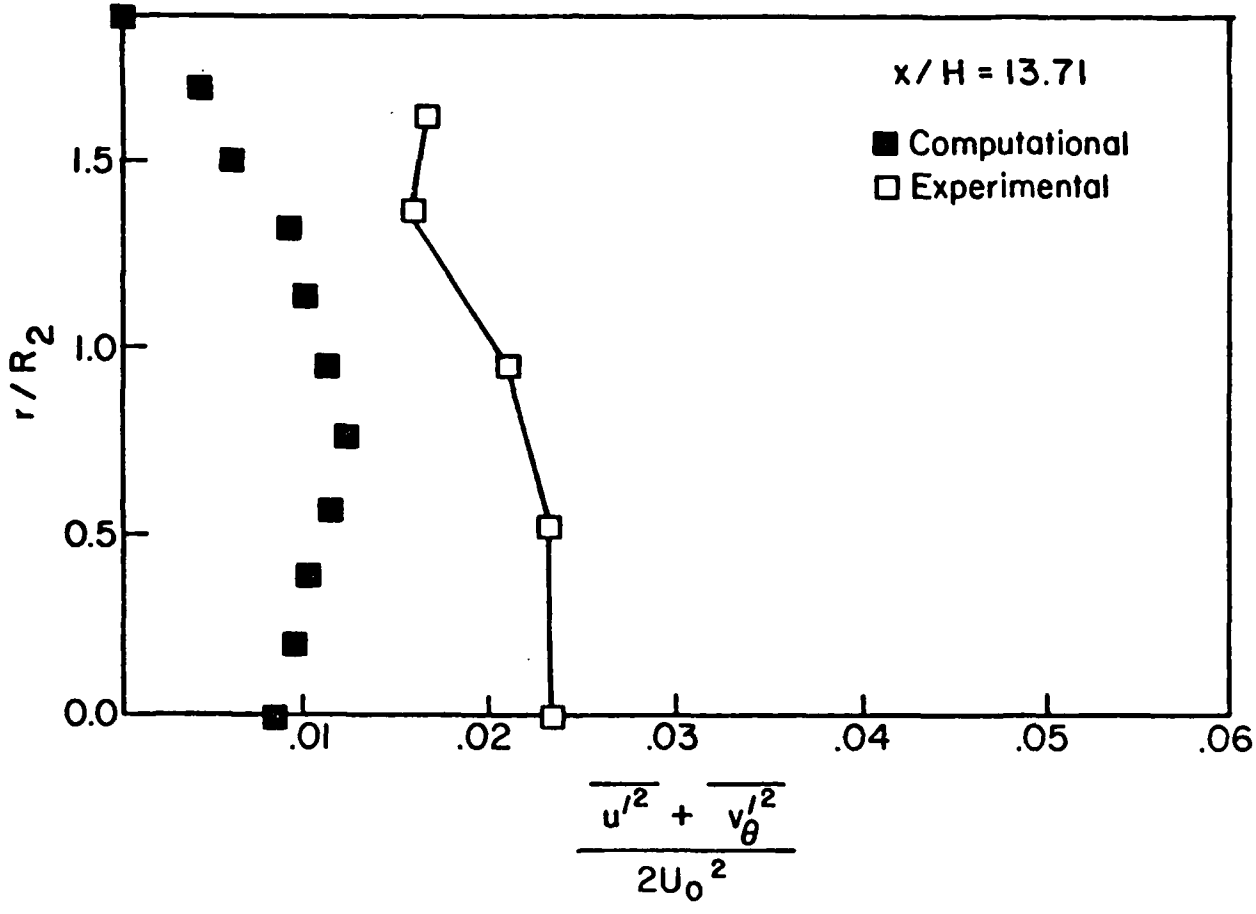

Figure 35 Comparison of predicted and measured turbulent kinetic energy at x/H=13.71

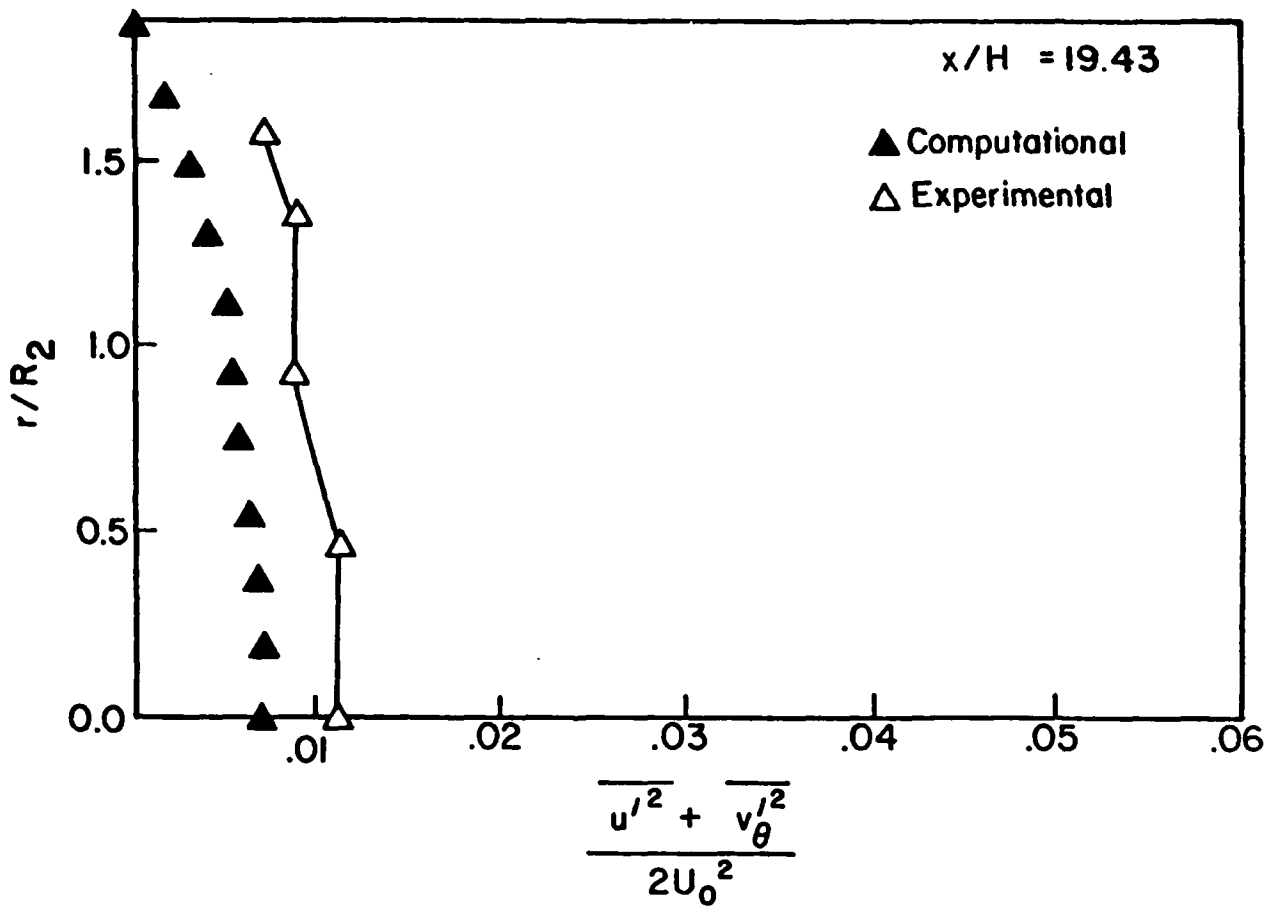

Figure 36 Comparison of predicted and measured turbulent kinetic energy at x/H=19.43

SECTION VI

CONCLUSIONS AND RECOMMENDATIONS

Several conclusions can be drawn from the flow information gathered in this study. The high turbulence level on the centerline seems to indicate that the flow downstream of reattachment is more active than one might suspect, even though the mean velocity data shows the expected flow pattern. This may indicate that although the flow at the inlet to the sudden expansion is steady, mean velocity fluctuations may be occuring downstream. Further study is needed to resolve this problem.

It was shown that accurate values for mean and RMS velocities can be obtained from direct LDV measurements although some loss of accuracy probably occurs when several direct measurements are input into the equations of Logan (SECTION IV) to calculate other turbulence parameters. In spite of the question of quantitative accuracy, qualitatively this flow data is still quite useful. Simultaneous measurements of the velocity components with a two component LDV are needed to examine the absolute accuracy of these results.

An experimental study of the effect of particle velocity on Doppler signal amplitude was made to determine if such an effect would compensate for velocity bias. No such effect was found over a large velocity range. This result leads one to doubt whether the phenomenon really exists.

The k-ε turbulence model used in the computer code CHAMPION 2/E/FIX produced results in overall fair agreement with the experimental

measurements. The major deficiences in this code are the lack of conservation of mass, which probably led to the poor performance in predicting the mean centerline velocity decay, and perhaps the manner in which the exit boundary condition is input. Although there were some quantitative discrepencies, the code yielded a useful qualitative description of the flow field.

Some areas which need further investigation and could prove to be quite helpful in the development of the LDV and the description of this flow field are:

1. The development of correction lenses which would allow off-axis measurements and thus yield radial flow information.
2. The modification of the 2/E/FIX code to more accurately describe the flow field downstream of a sudden expansion.
3. The development of alternate methods of obtaining bias-free data which relax the requirement of high signal validation rates.

LIST OF REFERENCES

[1] Macagno, E. O., and Hung, T. K., "Computational and Experimental Study of a Captive Annular Eddy," Journal of Fluid Mechanics, Vol. 28, pt. 1, pp. 43-63, 12 April, 1967.

[2] Zemanick, P. P., and Dougall, R. S., "Local Heat Transfer Downstream of an Abrupt Circular Channel Expansion," ASME Journal of Heat Transfer, Vol. 92, pp. 53-60, February, 1970.

[3] Back, L. H., and Roschke, E. J., "Shear-Layer Flow Regimes and Wave Instabilities and Reattachment Lengths Downstream of an Abrupt Circular Channel Expansion," ASME Journal of Applied Mechanics, Vol. 94E, pp. 677-681, September, 1972.

[4] Teyssandier, R. G., and Wilson, M. P., "An Analysis of Flow through Sudden Enlargments in Pipes," Journal of Fluid Mechanics, Vol. 64, pt. 1, pp. 85-95, June, 1974.

[5] Freeman, A. R., "Laser Anemometer Measurements in the Recirculating Region Downstream of a Sudden Pipe Expansion," In Proceedings of the LDA-Symposium Copenhagen, pp. 704-709, 1975.

[6] Gosman, A. D., Khalil, E. E., and Whitelaw, J. H., "The Calculation of Two-Dimensional Turbulent Flows," Turbulent Shear Flows I, Springer-Verlag, New York, pp. 13.35-13.45, 1977.

[7] Drewry, J. E., "Fluid Dynamic Characterization of Sudden-Expansion Ramjet Combustor Flowfields," AIAA Journal, Vol. 16, No. 4, pp. 313-319, April, 1978.

[8] Moon, L. F., and Rudinger, G., "Velocity Distribution in an Abruptly Expanding Circular Duct," ASME Journal of Fluids Engineering, Vol. 99, pp. 226-230, March, 1977.

[9] Kangovi, S., and Page, R. H., "Subsonic Turbulent Flow Past a Downstream Facing Annular Step," ASME Journal of Fluids Engineering, Vol. 101, pp. 230-236, June, 1979.

[10] Kuehn, D. M., "Effects of Adverse Pressure Gradient on the Incompressible Reattaching Flow over a Rearward-Facing Step," AIAA Journal, Vol. 18, No. 3, pp. 343-344, March, 1980.

[11] Roesler, T., Stevenson, W. H., and Thompson, H. D., "Investigation of Bias Errors in Laser Doppler Velocimeter Measurements," AFWAL-TR-80-2108, December 1980.

[12] McLaughlin, D. K., and Tiederman, W. G., "Bias Correction for Individual Realization Laser Anemometry Measurements in Turbulent Flows," Physics of Fluids, Vol. 16, No. 12 (1973), p. 2082.

[13] Barnett, D., and Bentley, H., "Statistical Bias of Individual Realization Laser Velocimeters," Proceedings of the Second International Workshop on Laser Velocimetry, Purdue University, pp. 428, 1974.

[14] Hoesel, W., and Rodi, W., "New Biasing Elimination Method for Laser Doppler Velocimeter Counter Processing," Review of Scientific Instruments, Vol. 48, No. 7, pp. 9.0, 1977.

[15] Dimotakis, P. E., "Single Scattering Particle Laser Doppler Measurements of Turbulence," Proceedings of the ISL/AGARD Workshop on Laser Anemometry, German-French Research Institute, St-Louis, France, pp. 189, 1976.

[16] Durão, D. F. G., Laker, J. and Whitelaw, J. H., "Bias Effects in Laser Doppler Anemometry," Journal of Physics E, Vol. 13, pp. 442, 1980.

[17] Durão, D. F. G., and Whitelaw, J. H., "Relationship Between Velocity and Signal Quality in Laser Doppler Anemometry," Journal of Physics E, vol. 12, pp. 47, 1979.

[18] McDougall, T. J., "Bias Correction for Individual Realization LDA Measurements," Journal of Physics E, Vol. 13, pp. 53, 1980.

[19] McVey, R., "The Design of a Laser Doppler Velocimeter for use in Studying Turbulent and Mixing Flows," Master's Thesis, Purdue University, 1979.

[20] Instruction Manual for TSI Model 1980 Counter, Thermo-Systems Incorporated, St. Paul, Minnesota.

[21] Logan, S. E., "A Laser Velocimeter for Reynolds Stress and Other Turbulence Parameters," AIAA Journal, Vol. 19, No. 7, pp. 933-935, 1972.

[22] Logan, S. E., "A Laser Velocimeter for Reynolds Stress and Turbulence in Dilute Polymer Solutions," Ph.D. Thesis, California Institute of Technology, 1972.

[23] Bremmer, R., Thompson, H. D., Stevenson, W. H., "An Experimental and Numerical Comparison of Turbulent Flow Over a Step," AFWAL-TR-80-2105, December 1980.

[24] Pun, W. M. and Spalding, D. B., "A General Computer Program for Two-Dimensional Elliptic Flows," Imperial College Mechanical Engineering Department Report N. HTS/76/2.

[25] Launder, B. E., and Spalding D. B., "The Numerical Computation of Turbulent Flows," Computer Methods in Applied Mechanics and Engineering, Vol. 3, 1974, p. 269.

APPENDIX

Data Analysis

All data analysis was performed using a Fortran program on the Purdue University Computing Center's CDC 6500 and 6600. The program consists of a main routine and four subroutines.

The main routine reads a data file from a disk consisting of m points with three digital numbers per point, n (exponent), N (cycles/burst), Dm (digital mantissa), and converts it to a frequency using

$$f_i = \frac{N \times 10^9}{D_m \times 2^{n-2}} \tag{A1}$$

The Doppler frequency, F, is then used to calculate a velocity using

$$V_i = [\text{sign } (f_i) - f_s] \, F_R \tag{A2}$$

where f_i is the Doppler frequency, f_s is the frequency shift (negative for fringes moving in the same direction as the flow), sign is positive for positive frequency shifting and negative for a negative frequency shift and F_R is the fringe spacing.

The fringe spacing is determined using the experimental set up in Figure A1 and the following equations.

$$\frac{\theta}{2} = \tan^{-1} \frac{x/2}{y} \tag{A3}$$

$$F_R = \lambda/2 \sin(\theta/2) \tag{A4}$$

where $\theta/2$ is the beam half angle, λ is the wavelength of the laser light, x and y are distances shown in Figure A1 and F_R is the fringe spacing.

Once velocities for the m frequencies have been computed, the main routine calls subroutine STATS. STATS performs all of the statistical manipulations in the computer program. This subroutine computes the mean velocity, $\bar{U}$, the variance $(\overline{u'^2})^{1/2}$, the standard deviation, $(\overline{U'^2})^{1/2}$, the standard deviation from the mean, T_m, and the skewness coefficient, s, as given by the following equations:

$$\bar{U} = \frac{1}{m} \sum_{i=1}^{m} U_i \tag{A5}$$

$$\overline{u'^2} = \frac{1}{m} \sum_{i=1}^{m} (U_i - \bar{U})^2 \tag{A6}$$

$$(\overline{u'^2})^{1/2} = \left[\frac{1}{m} \sum_{i=1}^{m} (U_i - \bar{U})^2\right]^{1/2} \tag{A7}$$

$$T_m = \left(\frac{\overline{u'^2}}{m}\right)^{1/2} \tag{A8}$$

$$S = \frac{\frac{1}{m} \sum_{i=1}^{m} (U_i - \bar{U})^3}{[(\overline{u'^2})^3]^{1/2}} \tag{A9}$$

STATS also calculates corrected mean velocities and standard deviations using McLaughlin and Tiederman's one-dimensional correction scheme. One of the problems with this correction scheme is that when $U_i \to 0$, $\frac{1}{U_i} \to \infty$. This problem was eliminated by using ensemble averaging for velocities between .1 and -.1 m/s and using the correction scheme for all other velocities. The two means were then weighted by the number of points

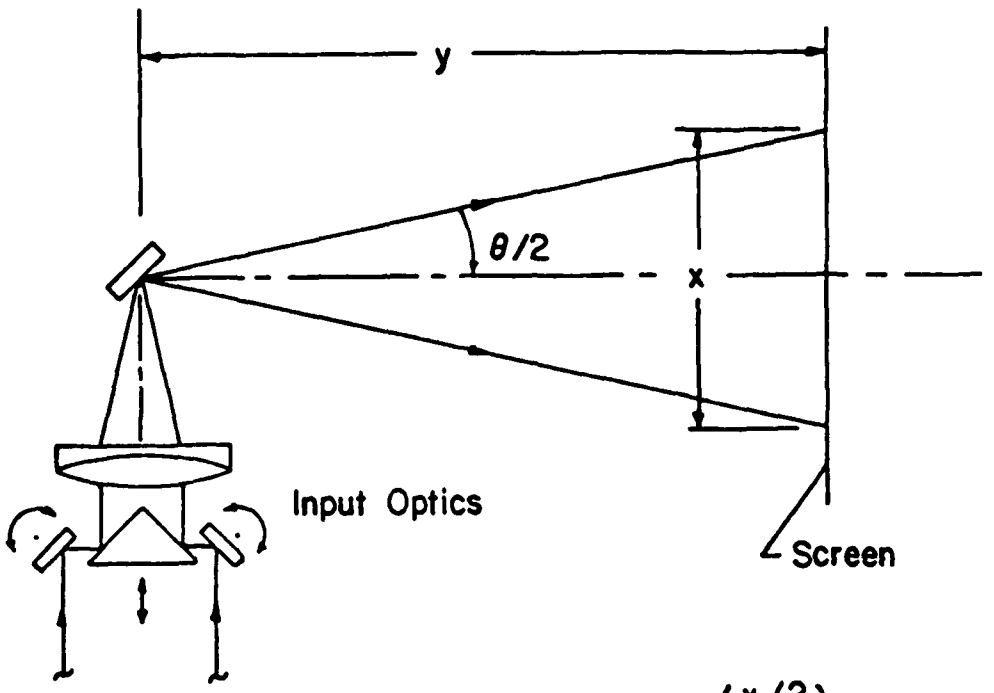

$$\theta/2 = \tan^{-1}\left(\frac{x/2}{y}\right)$$

Figure A1 Arrangement for measuring beam angle

in each group and averaged together to obtain the corrected mean velocity.

A histogram of the raw data is then plotted using subroutines HIST and USHV1. The program also contains a data editing subroutine called SELECT. SELECT edits the raw data using one of three methods. The first method allows for the discarding of data points which are beyond a specified number of standard deviations from the mean. The second allows the user to set the maximum and minimum velocities to be used in the statistical manipulations. The third method allows the user to set a specific number of bins in the histogram. Bins at the end of the histogram which do not contain a specified number of velocity realizations are discarded. After editing the program calls STATS, HIST and USHV1 again to determine the revised statistical quantities and plot the revised histogram. In the present study a 3T cutoff was used in SELECT for all data editing. Typical histograms before and after editing are shown in Figures A2 and A3 respectively.

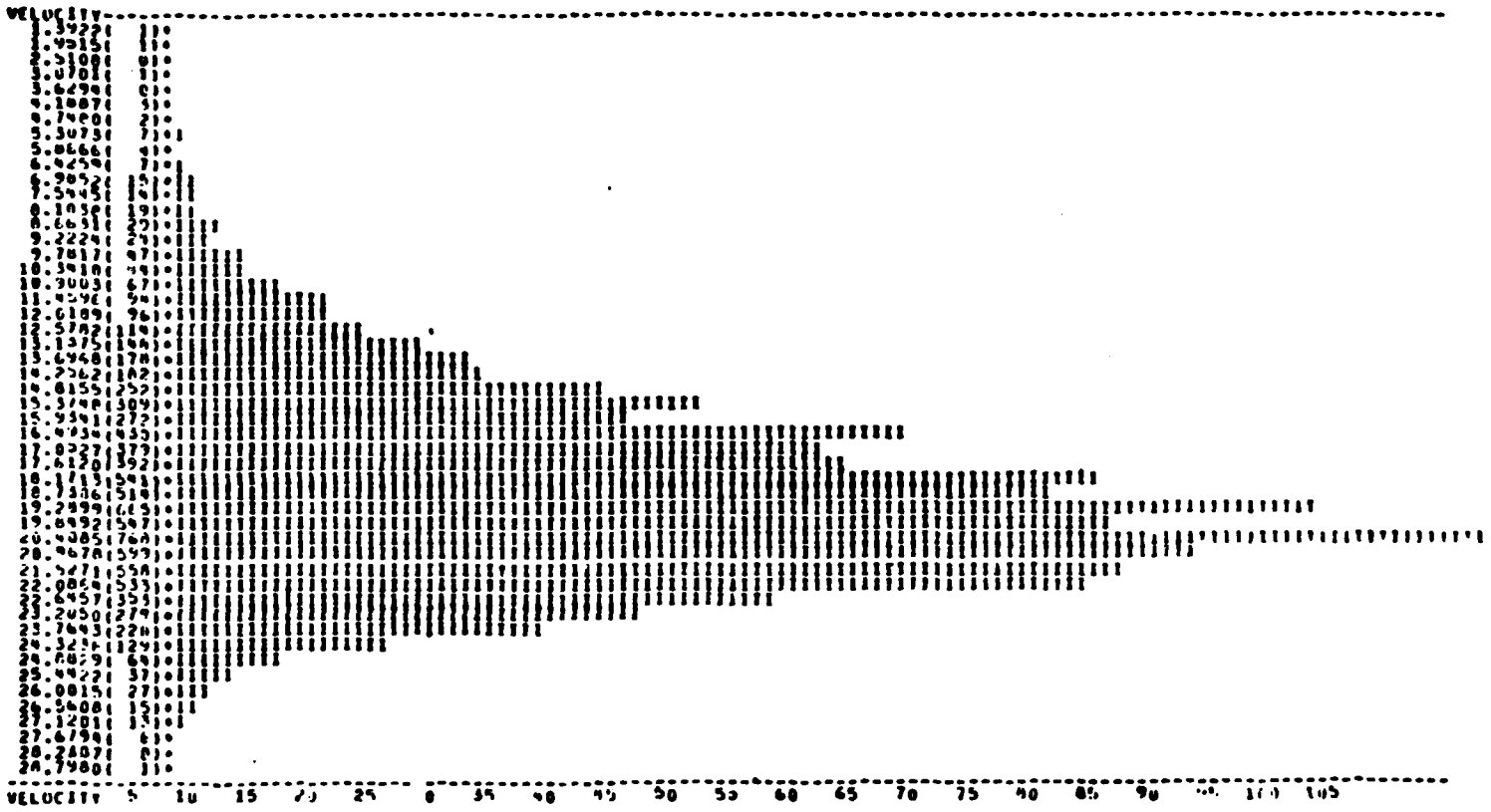

Figure A2 Sample histogram before editing

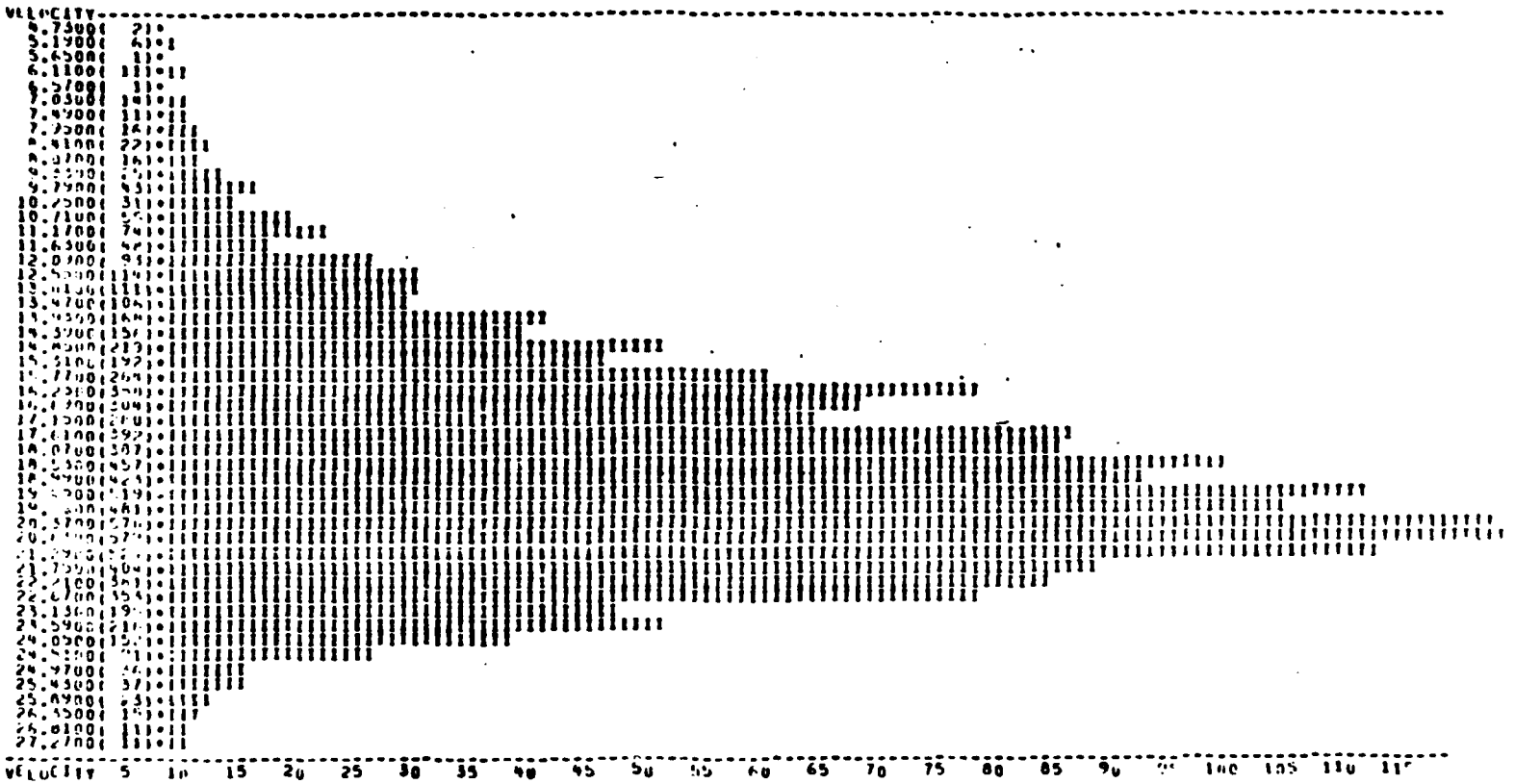

Figure A3 Sample histogram after editing